Accepted Manuscript

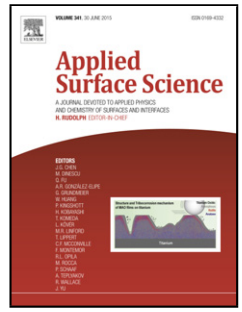

Title: XPS and FTIR Spectroscopic Study on Microwave Treated High Phosphorus Iron Ore

Author: Mamdouh Omran Timo Fabritius Ahmed M. Elmahdy Nagui A. Abdel-Khalek Mortada El-Aref Abd El-Hamid Elmanawi

PII: S0169-4332(15)00825-9
DOI: http://dx.doi.org/doi:10.1016/j.apsusc.2015.03.209
Reference: APSUSC 30086

To appear in: *APSUSC*

Received date: 11-2-2015
Revised date: 25-3-2015
Accepted date: 30-3-2015

Highlights

- The effect of microwave radiation on structure and chemical state of high phosphorus iron ore was studied.
- FTIR analyses showed that after microwave radiation the functional chemical groups of phosphorus bearing minerals (fluorapatite) dissociated.
- High resolution XPS analyses of Fe 2p peaks showed that after microwave radiation a portion of Fe (+III) was reduced to Fe (+II).
- Microwave radiation had a positive effect on the magnetic properties of iron oxide, through formation of ferromagnetic phases.

XPS and FTIR Spectroscopic Study on Microwave Treated High Phosphorus Iron Ore

Mamdouh Omran[a,b*], Timo Fabritius[a], Ahmed M. Elmahdy[b], Nagui A. Abdel-Khalek[b], Mortada El-Aref[c], Abd El-Hamid Elmanawi[c]

[a] Process Metallurgy Research Group, Faculty of Technology, University of Oulu, Finland.

[b] Mineral Processing and Agglomeration Lab, Central Metallurgical Research and Development Institute, Cairo, Egypt.

[c] Geology Department, Faculty of Science, Cairo University, Giza 12613, Egypt.

Abstract:

A growing interest in microwave heating has emerged recently. Several potential microwave applications regarding minerals' processing have been investigated. This paper investigates the effect of microwave radiation on Egyptian high phosphorus iron ore. Three different iron ore samples have varying Fe_2O_3 and P_2O_5 contents and mineralogical textures were studied. A comparative study has been carried out between untreated and microwave treated iron ore. XRD and FTIR analyses showed that after microwave radiation the crystallinity of iron bearing minerals (hematite) increased, while the functional chemical groups of phosphorus bearing minerals (fluorapatite) and other gangues dissociated. High resolution XPS analyses of Fe 2p peaks showed that after microwave radiation a portion of Fe (+III) was reduced to Fe(+II). This means that after microwave radiation iron oxide (hematite, Fe^{3+}) transformed into more magnetic phase. The results indicated that microwave radiation had a positive effect on the magnetic properties of iron oxide, through formation of ferromagnetic phases.

Kew words: High phosphorus iron ore; Microwave treatment; XPS; FTIR.

Corresponding author:

Mamdouh Omran

Present address: Process Metallurgy Research Group, Faculty of Technology, University of Oulu, Finland. P.O. Box 4300.
E-mail: mamdouh.omran@oulu.fi

Introduction

Microwave energy is a non-ionizing electromagnetic radiation with frequencies in the range of 300 MHz to 300 GHz. Microwave frequencies include three bands: ultra-high frequency (UHF: 300 MHz to 3 GHz), super high frequency (SHF: 3 GHz to 30 GHz) and extremely high frequency (EHF: 30 GHz to 300 GHz) [1, 2]. Microwave heating is fundamentally different from conventional heating because microwaves take the form of electromagnetic energy and can penetrate deep into the sample. This allows sample heating to be initiated volumetrically, as opposed to conventional thermal processing which heats the sample from the outside inward via standard heat transfer mechanisms, i.e., through convection, conduction, and radiation [3]. Compared with conventional heating techniques, the main advantages of microwave heating are: non-contact heating, energy transfer rather than heat transfer, rapid heating, material selective heating, lower power consumption and volumetric heating [2, 3].

Omran et al. [4] investigated the influence of microwave radiation on the magnetic properties and magnetic separation of iron ore. The results indicated that the improvement in iron recovery is attributed to microwave radiation enhancement of the magnetic properties of weak magnetic mineral (hematite) through altering the mineral to more magnetic phases (maghemite or magnetite). The influence of microwave pre-treatment on the liberation of high phosphorus oolitic iron ore was also investigated [5, 6]. The results showed that compared to conventional thermal treatment, microwave treatment consumes considerably less energy, improves liberation and reduces processing time.

Guo Chen et al. [7, 8, 9] investigated the influence of microwave pre-treatment on magnetic separation and surface characteristics of ilmenite ores. Chen et al. concluded that microwave treatment of ilmenite ore is potentially high efficient pre-treatment technique for magnetic separation with low energy consumption. The influence of microwave irradiation on the grindability of gold ores was investigated [10]. It was concluded that microwave assisted grinding produced good results particularly for grinding characteristics.

In order to obtain detailed information about the effect of microwave radiation on iron ore, X-ray photoelectron spectroscopy (XPS) is employed. XPS is a highly surface sensitive technique that can be used for compositional and chemical states analysis [11]. This technique provides information about the oxidation and structural states of the iron oxides.

For the analysis of photoelectron spectra of iron oxides, peak shape and peak binding energy comparisons to standard compounds are used to derive oxide composition. For qualitative iron oxide determination McIntyre and Zetaruks [12] studied the XPS spectra of the simple and mixed iron oxides, the details of core line spectra (Fe (2p), Fe (3s), Fe (3p), and O (ls)), valence band spectra, and Auger line spectra are used to identify features which allow identification of each species. Comparative study of iron oxide XP spectra has been made by Allen et al. [13] who obtained Fe (2p) and O (1s) spectra of αFe_2O_3, Fe_3O_4, FeO, αFeOOH, and several ferrates. They found that the Fe (2p) spectra were particularly difficult to analyze, because of a steeply rising background and broadened line widths. They attributed such broadening to multiplet splitting and shake-up phenomena. Mekki et al. [14] used the Fe 3p spectra to obtain quantitative information on Fe^{2+} and Fe^{3+} concentrations in silicate glass samples. The Fe^{2+} and Fe^{3+} ions were assumed to generate overlapping Fe 3p spectra. These peaks were deconvoluted into two peaks to obtain the Fe^{2+} and Fe^{3+} ratios. Grosvenor et al. [15] various iron oxide, hydroxide and halide have been analyzed by XPS and peak shapes fitted with a close approximation of the Gupta and Sen [16] multiplet structure. They concluded that all Fe (II) and Fe (III) species can be fitted with Gupta and Sen multiplet structure.

The aim of this study is to investigate the effect of microwave radiation on the structure and chemical state of high phosphorus iron ore using different techniques.

Materials and Methods

Materials

The iron ore samples used in this study were collected from Aswan region, Egypt. Eastern Aswan area represents the main occurrence of the Cretaceous ironstone bands of South Egypt, which are confined to clastic successions belonging to the “Nubian” sandstones or “Nubia facies” [17, 18]. Three different samples were obtained from different locations from Aswan region. Fig. (1) and Table (1) present the XRD patterns and chemical analysis, respectively, of the iron ore samples investigated in this study. The following mineral phases were found, for all samples, hematite is the main iron bearing minerals. In addition to quartz, fluorapatite and chamosite as gangues. These samples have different mineralogical texture, and Fe_2O_3 and P_2O_5 percentage. Based on the chemical compositions and sample texture, the iron ore samples are classified into three types:

1. Sample with Fe_2O_3 (62.18 %) and P_2O_5 (5.64 %), sample G1
2. Sample with Fe_2O_3 (59.28 %) and P_2O_5 (2.25 %), sample G2
3. Sample with Fe_2O_3 (74.96 %) and P_2O_5 (3.24 %), sample G3

Sample G3, SEM images show that Fe-bearing minerals occur mainly as ooiltic hematite more than 95 % (Fig. 2A and 2B). Fluoroapatite and chamosite occur as fine-grained filling the spaces between oolitic grains (Fig. 2B, 2C and 2D). Sample G2, Figure (2E) show that sample composed mainly from ooiltic hematite about 50 % and detrital quartz. Sample G1, SEM images show that Fe-bearing minerals occur mainly as fine-grained cement-like materials mixed with phosphorus bearing mineral (Fig. 2F and 2H).

Microwave treatment

Samples were treated using a 2.45 GHz microwave oven (sandstorm, model S25CSS11E and cavity dimension 513 mm (D) × 482 mm (W) × 310 mm (H)) with 900 W maximum output power. Iron ore samples were treated in the oven for varying exposure times. 100 grams of the representative samples with grain size in the range (-2mm +1mm) were used in each test. Iron ore samples were treated under normal atmosphere condition and directly used without any pretreatment. Samples were placed in the microwave oven in crucibles made of pure alumina. The temperature of each sample was measured by quickly inserting a thermocouple into the sample after the power was turned off, and the temperature was monitored by a digital display temperature controller. The measured temperatures are the bulk temperature of the samples (Table 2). The samples were then allowed to cool in the microwave oven to room temperature.

Analytical techniques

X-ray diffraction (XRD) & X-ray fluorescence (XRF)

The bulk mineralogical composition and crystallinity of the iron ore samples were performed on powdered samples using a Siemens D5000 XRD powder diffractometer. The device contains a Cu Kα radiation with a graphite monochromator. The XRD analyses were made using 40 KV and 40 mA. Chemical analyses were performed on whole rock powders by X-ray fluorescence (Bruker AXS S4 Pioneer).

Scanning Electron Microscope (SEM)

The micro-morphological characteristics of the iron ore before and after microwave treatment were investigated using Zeiss ULTRA plus field emission scanning electron microscope (FESEM) attached to an Energy dispersive X-ray spectroscopy (EDS) unit for chemical analysis.

Thermoanalyses (TG-DSC) & Mass spectroscopy (MS)

The thermal behavior of iron ore was studied using thermogravimetry (TG–DSC) and mass spectroscopy (MS), which was performed using a Netzsch STA409 PC Luxx under air atmosphere. Approximately 30.84 mg of sample was placed in a platinum crucible on a pan of the microbalance at a heating rate of 20 °C/min. The temperature range was 20–1250 °C.

Fourier Transform Infrared (FTIR) spectroscopy

Infrared Spectroscopy is used for the identification of iron oxide and provides information about crystal morphology, degree of crystallization of iron oxide. Surface chemistry of microwave treated and untreated samples were examined via Bruker Vertex V80 vacuum FT-IR spectrometer with Harrick Praying Mantis TM DRIFT equipment. The angle of incidence of the IR beam was 45° and 100 scans were collected at a resolution of 4 cm^{-1}. The spectral were collected within the range of 4000–400 cm^{-1} wave number.

X-ray photoelectron spectroscopy (XPS)

X-ray photoelectron spectroscopy was used to provide information about the oxidation and structural state of the iron oxides. The X-ray photoelectron spectroscopy was carried out using an ESCALAB 250Xi instrument manufactured by Thermo Fisher Scientific. We used monochromatic Al Ka line radiation, the base pressure of the analysis chamber before the experiment was about $1x10^{-9}$ mbar. During the measurement the pressure was about $4x10^{-7}$ mbar due to the surface charge compensation system. All binding energies were calibrated using C 1 s peak with a fixed value of 284.8 eV. Samples were prepared as compressed powder on pieces of indium. Indium was selected because of its softness that gives a mechanical consistency to the sample and its electrical conductivity, which is adapted to the analysis of insulating or semi-conductive materials. Spectra were analyzed using Avantage software (version 5.934). Spectra of iron, and oxygen were fitted using a Shirley background, and line shapes were expressed by an asymmetric Gaussian–Lorentzian sum function. The Fe $2p_{3/2}$ envelope was fit using peaks corresponding to the GS multiplets [16] and Grosvenor et al. [15].

Results and discussion

Thermoanalyses (TG-DSC) & Mass spectroscopy (MS)

Thermogravimetry (TG) and differential scanning calorimeter (DSC) analyses are shown in Figs. (3, 5 and 5). In sample G1 (Fig. 3) three endothermic peaks (73 °C, 292 °C and 494 °C) and weak exothermic peak (574 °C) were found during the heating process. In sample G2 (Fig. 4) two endothermic peaks (64 °C and 568 °C) and weak exothermic peak (682 °C) were found during the heating process. In sample G3 (Fig. 5), three endothermic peaks (74 °C, 276 °C and 483 °C) and two weak exothermic peaks (521 °C and 615 °C) were found during the heating process.

In all samples, the endothermic peaks resulted from moisture evaporation and the removal of free and combined water that are associated with the series of weight losses shown in Figs. (3a, 4a and 5a). This behavior was confirmed by the results of mass spectrometry for the H_2O evolved during the heating process (Figs. 3b, 4b and 5b). There are weak exothermic reactions between 616 °C and 680 °C, probably due to the recrystallization of the carbonate-apatite (fluoroapatite); this recrystallization involves the release of CO_2 from carbonate-apatite structure. This release of CO_2 was observed in mass spectrometry for CO_2 gas evolving during heating process (Figs. 3b, 4b and 5b). The DTG curve shows a slight weight loss between 616 °C and 680 °C (Fig. 5b), which confirms the release of CO_2 in this temperature range.

X-ray diffraction (XRD)

The effect of microwave radiation on the crystal structure of iron ore was characterized by XRD. Figs. (6, 7 and 8) show the XRD analysis for untreated iron ore and iron ore exposed to 900 W microwave power for a durations of 60 s and 120 s.

In sample G1 (Fig.6), At 60 s of exposure time, the peak intensity of hematite increases in the microwave-treated sample, while the peak of goethite disappeared, due to transformation of goethite to hematite. At this exposure time, water removed from goethite. There are change in the peak of fluorapatite due to the recrystallization of the carbonate-apatite (fluorapatite) and release of CO_2 from carbonate-apatite structure as indicated in TG-DSC analysis. At 120 s of microwave exposure time, the peaks of phosphorus bearing mineral (fluorapatite) completely gone out, which indicated that fluorapatite decomposed at this exposure time and become amorphous. Also traces of ferromagnetic (maghemite or magnetite) were observed.

In sample G2 (Fig.7), with increasing microwave exposure time, the peak of hematite become sharper. At 120 s of exposure time, traces of ferromagnetic (maghemite or magnetite) were observed.

In sample G3 (Fig.8), At 60 s exposure time, the microwave-treated sample exhibits peaks that are sharper than that of the untreated sample. This behavior indicates that the peak intensity of hematite increases after microwave treatment, but no phase change occurs. In addition, the peak of chamosite disappeared in the microwave-treated sample exposed for 60 s. Because the temperature of the sample at this exposure time was approximately 546 °C, chamosite decomposed at this temperature and became amorphous. At 120 s of microwave exposure, traces of ferromagnetic (maghemite or magnetite) were observed, which is due to a microwave-heating induced phase change at the grain boundaries of the minerals [19, 20]. Paramagnetic hematite (α - hematite) remains the dominant mineral phase. Fig. (9) indicates that after microwave treatment for 120 s, melting occurred at the grain boundaries of the mineral particles.

An explanation for the increasing hematite peak intensity with increasing microwave exposure time is that gangues were dissociated after exposure to microwave radiation, while the crystallinity of hematite was increased [7]. Barani et al. [21] observed the effect of microwave treatment on the crystal structure of iron ore. He found that after exposure to 1100 W of microwave radiation for 180 s, the XRD analysis indicated that the height of the peaks change with the microwave treatment, but no phase change occurred. This result due to the fact that any changes that occurred in the sample were below the threshold of the XRD sensitivity, which is approximately 5% of the sample volume [21].

Fourier Transform Infrared (FTIR) spectroscopy

The original iron ore sample and microwave treated samples were characterized using FTIR. Figs. (10a, 11a and 12a) illustrate the FTIR spectra of untreated iron ore samples. FTIR spectra of samples showed that the absorption band at a high wavenumber region is due to OH stretching, and at lower wavenumber as a result of Fe-O lattice vibration.

The IR bands of the studied samples at 408-428 cm^{-1}, 503-509 cm^{-1} and 701-709 cm^{-1} are considered to represent hematite [22, 23, 24]. All samples contain the characteristic OH stretching (νOH) and HOH bending (δOH) vibrational bands at 3423-3444 cm^{-1} and 1641.1 cm^{-1}, respectively [24, 25, 26]. These bands were reported in pure iron oxides [27, 28]. The broad absorption band around 3423.4 cm^{-1} (Fig. 10a) was attributed to stretching of hydroxyl of goethite and 'loosely bound water' adsorbed on the surface [29]. The bands at 3619, 3652, 3694 and 3696.9 cm^{-1} correspond to bridging OH groups in Al-OH-Si and can be attributed to the location of hydrogen atom(s) on different oxygen atoms in the framework [30]. It was observed that weak tiny complex bands at 1000−1100 cm^{-1}, these bands can be assigned to the asymmetric stretch vibration of the phosphate group (Fig. 10a). In addition, doublet bands at 1429-1430 cm^{-1} and 1529-1554 cm^{-1} correspond to carbonate group, which is related to phosphorus bearing minerals [31] Figs. (10a, 12a). Bands in region from 815-1119 cm^{-1} and 1878-1995 cm^{-1} (Fig. 11a), bands from 1087-1182 cm^{-1} and 1787-1999 cm^{-1} (Fig. 10a), band at 1083 cm^{-1} (Fig. 12a) due to quartz (SiO_2) grains.

The FTIR spectrum of the microwave treated iron ore for 60 s is shown in Figs. (10b, 11b and 12b). The most obvious change in the spectrum is that the bands at 1641 cm^{-1}, 3423-3444 cm^{-1} and 3696.89 cm^{-1} gradually decreased due to the removal of free and combined water from the sample after microwave treatment. The occurrence of a new band in FTIR spectra from 2343 to 2360 cm^{-1} is attributed to adsorbed atmospheric carbon dioxide on the sample surface [25].

The FT-IR spectrum of microwave treated iron ore for a duration of 120 seconds can be seen from Figs. (10c, 11c and 12c). The bands attributed to the O–H stretching mode and H–O–H bending mode, and bands attributed to phosphate and carbonate groups, which are related to phosphorus bearing minerals, of the original iron ore disappeared. A possible explanation is that after microwave radiation the functional chemical groups of phosphorus bearing mineral and other gangues have dissociated [7]. Due to selective heating of microwave, based on dielectric properties of materials, iron oxides is good heated with microwave while gangues (carbonates, phosphates and silicates groups) are little heated with microwave, hereby after microwave radiation the crystallinity of iron bearing minerals increase and the functional chemical group of gangue dissociated after microwave radiation due to interact mineral matter with gangue [7].

X-ray photoelectron spectroscopy (XPS)

XRD and FTIR didn't give enough or detailed information about the effect of microwave radiation on iron bearing minerals. In order to obtain information about the oxidation state and structure of iron bearing minerals, high resolution spectra of Fe (2p) peak and the O (1s) peak were studied.

XPS survey scans of high phosphorus iron ore indicated the presence of Fe, O, Si, Ca and P (Figs. 13- 15). It can be seen that the shift in the Fe (2p) peak binding energy corresponds to iron oxide as a main component of the iron ore whereas the shift in the O (1s) peak corresponds to oxygen, phosphate and iron oxides speciation. Also, the shifts in the Ca (2p) and P (2p) peaks correspond to phosphate mineral, and the shift in the Si (2s) peak corresponds to quartz.

Figs. (13, 14 and 15a&b) show the XPS survey scan spectra of untreated and microwave treated samples for 120 s, respectively. These figures demonstrate insignificant difference between untreated and microwave treated samples except the Ca (2p) peak which is slightly increased in the intensity of Ca (2p) peak after microwave treatment, which can be attributed to fluorapatite decomposition after microwave treatment.

Fe 2p spectra

Figs. 16, 17 and 18 show the Fe 2p core level XPS spectra of untreated and microwave treated samples for 120 s, recorded for a narrow scan between 695.0 eV and 745.0 eV.

For untreated sample (Figs. 16 - 18), the Fe 2p spectrum contain two peaks of Fe $2p_{3/2}$ and Fe $2p_{1/2}$ at binding energy (B.E.) positions of ~710.28 - 710.48 eV and ~723.78 – 723.88 eV, respectively.

The observed signals at these B.E. positions seem to correspond to the formation of iron oxide phase, i.e., Fe^{3+} in Fe_2O_3 (hematite) phase [32-37]. The Fe $2p_{3/2}$ peak has associated satellite peaks at ~718.28 – 718.48 eV. Researchers have investigated that the satellite peak of Fe $2p_{3/2}$ for Fe_2O_3 is located approximately 8 eV higher than the main Fe $2p_{3/2}$ peak [38-40]. In addition, another satellite peak at ~ 732.5 – 732.58 eV; this may be a satellite peak for Fe $2p_{1/2}$. The observed B.E.

difference between Fe 2p doublet spectra, i.e., between $2p_{3/2}$ and $2p_{1/2}$ is ~13.4 corresponding to iron oxide (Fe_2O_3) phase [34, 41, 42].

For microwave treated samples (Figs. 16 - 18), there is a significant shift in the position of the peak maxima in the Fe 2p doublet, the B.E. positions are observed to be at ~709.48 – 709.68 eV (for Fe $2p_{3/2}$) and ~722.98 eV (for Fe $2p_{1/2}$) which is shifted to lower B.E. side as compared to untreated samples. The satellite peak which associates with Fe $2p_{3/2}$ peak disappeared in microwave treated samples.

Figs. 16-18 show the fitted Fe $2p_{3/2}$ spectra for untreated and microwave treated samples for 120 s, respectively.

For untreated samples, (Figs. 16a -18a), the $2p_{3/2}$ envelopes have been fitted well with the GS multiplets, the multiplets and surface peaks used to fit the Fe^{3+} have been labelled on the spectrum. The fitted $2p_{3/2}$ envelopes correspond to the presence of iron oxide Fe^{3+}, i.e., Fe_2O_3 phase. A satellite peak is also observed at binding energy (B.E.) position ~718.28 – 718.48 eV which is ~8.0 eV higher than Fe $2p_{3/2}$ peak [12, 43-46].

On the microwave treated samples (Figs. 16b - 18b), the $2p_{3/2}$ spectrum is distinct from untreated samples, having a thick Fe $2p_{3/2}$ envelope with a shoulder on the low-BE side. A single low-intensity peak on the low-binding-energy (BE) side of the envelope was added to account for the formation of Fe ions with a lower oxidation state Fe^{2+} [15]. It can also be seen from the spectra that B.E. positions of Fe $2p_{3/2}$ get shifted to lower B.E. side on the microwave radiated samples. Satellite peak which associated with $2p_{3/2}$ disappeared on microwave treated samples. This means that the oxidation state of iron oxide has been changed.

The Fe $2p_{3/2}$ spectra for the untreated iron ore shows relatively narrow peaks (FWHM) of Ca. (3.8 – 3.9) with a small broad satellite peak centered around ~718.28 – 718.48 eV, that is typical of the Fe(III) oxidation state [12, 44]. When the sample treated with microwave, there was a significant broadening of the Fe $2p_{3/2}$ peak (FWHM) of Ca. (4.8 – 4.9) and it was shifted to a lower BE. This finding indicates the presence of a mixture of Fe(II) and Fe(III) oxides, both of which contribute to the Fe $2p_{2/3}$, some reduction of Fe^{3+} state to Fe^{2+}, has taken place. This means that after microwave radiation iron oxide (hematite, Fe^{3+}) transformed into more magnetic phase as observed due to reduction of some Fe^{3+} to Fe^{2+}. This finding confirmed by other researchers [13, 44, 47, 48]. This result was investigated by Omran et al. [4]. They concluded that the improvement in iron recovery is attributed to microwave radiation enhancement of the magnetic properties of weak magnetic mineral (hematite) through the altering of the paramagnetic hematite mineral to more magnetic phases. In addition, changes in the Fe 2p peak shape were observed together with alterations in the profile and position of the O 1s peak. Shake-up satellite peak which changes as the oxidation state of iron is altered, gives an indication about the oxidation state of iron.

Fe2p 3/2 satellite

The exploitation of charge transfer satellites (presence or absence, distance between a satellite and its photoelectron peak) associated to Fe 2p peaks gives data about the oxidation state of iron [34, 49, 50]. The positions of the satellite peaks for the Fe $2p_{1/2}$ and Fe $2p_{3/2}$ peaks are also very sensitive to the oxidation states and these peaks have been used for qualitatively determining the ionic states of iron [34]. These shake-up core -level satellites are caused by an incident x-ray photon giving up a discrete portion of its energy to the excitation of a second electron rather than imparting its entire quantum of energy to the primary, photo-ejected electron. This photoelectron will thus have lost a small amount of energy and will appear at a slightly higher binding energy than the parent peak [34].

In a compound in which iron is at the oxidation state (+II), satellite of Fe 2p constitutes a shoulder in the photoelectron peak, whereas for a species with Fe (+III), this same satellite is very distinctive from the photoelectron peak. Moreover, in mixed oxides of Fe (+II) and Fe (+III), such as Fe_3O_4, the charge transfer satellite has disappeared from the spectrum [34, 50, 51].

In the present study, for untreated samples, the $2p_{3/2}$ photoelectron peak is observed around 710.48 eV associated with a distinctive shake-up satellite around 718.48 eV. These features indicate that the iron found on the oxidation state Fe (+III). In the microwave treated samples, the $2p_{3/2}$ peak shifted to lower B.E. and the satellite peak has disappeared from the spectrum, which indicated that the iron found is a mixture of Fe(+II) and Fe(+III) oxidation states. These results indicated that after microwave radiation a portion of Fe(+III) was reduced to Fe(+II) and more magnetic phase was formed as investigated elsewhere [4]. These results indicated that microwave radiation had a positive effect on the magnetic properties of iron oxide, through the formation of ferromagnetic phases. This improvement in magnetic properties will facilitate the magnetic separation of iron bearing minerals from associated phosphate and other gangue minerals.

O1s spectra

Figs. (19 – 21) show the O 1s core level spectra of untreated and microwave treated samples for 120 s, recorded for a narrow scan between 525.0 eV and 545.0 eV.

The O1s spectrum for the untreated iron ore contains contributions from quartz, iron oxide, hydroxyl (OH -) and oxide oxygen (O^{2-}). Two main components are observed at (~529.48 – 529.98 eV) and (~531.28 – 532.08 eV). The lower binding peak due to the oxide [12, 34, 43, 44]. The second peak which occurs at higher binding energy due to the presence of hydroxyl species as a result of chemisorption of water on the air-exposed surfaces [44]. It was reported that O^{2-} oxygen shift to higher binding energies when OH- is structurally incorporated in the ferric oxide. They suggested that interaction between the proton on the hydroxyl oxygen and the oxide oxygen produces the binding energy shift to higher binding energies [12, 52].

Figs. (19 – 21) show the deconvoluted O 1s spectra of untreated and microwave treated samples for 120 s, respectively. Which shows differences between untreated and microwave treated iron ore samples.

The O 1s spectrum for sample G1 (Fig. 19) consists of two equal intensity O 1s peaks. The lower binding peak (529.48 eV) due to oxide, the second peak at (531.28 eV) due to hydroxyl. Microwave treatment shifted the oxygen peak to lower B.E. side by ~0.8 eV as compared to untreated sample.

The O 1s spectrum for sample G2 (Fig. 20) consists of two O 1s peaks. High intensity peak at (529.98 eV) due to oxide, and a low intensity peak at (532.08 eV) which is formed from hydroxyl component. After microwave treatment the oxygen peak getting shifted to lower B.E. side by ~0.8 – 0.9 eV as compared to untreated sample. It can be seen that, the shift in O 1s peaks to lower binding energy associated with the shift in Fe 2p peaks, due to reduction of some Fe^{+3} that transformed to Fe^{+2}.

The O 1s spectrum for sample G3 (Fig. 21) consists of two O 1s peaks. High intensity peak at (529.78 eV) due to oxide, and low intensity high energy tail at binding energy of (531.58 eV) which is formed from hydroxyl component. After microwave treatment, it can be seen that the high energy peak has completely gone out and a broad peak at ∼530.38 eV has been observed which is mainly

due to the oxide phase of iron (Fe^{+2} and Fe^{+3}).

The relative intensity of oxide and hydroxyl components vary with microwave treatment of iron ore where the O-H component drops significantly with microwave treatment, which causes the loss of water [12, 44, 47]. This phenomenon has been also evidenced by FTIR. Significant changes occur in the oxygen peak width, peak position and peak intensity associated with alterations in the Fe 2p profiles after microwave treatment, as shown in Figs. 19 - 21, indicated that a more ordered structure is developing. The disappearance of the high binding energy side of the O 1s peak is shown in Fig. 21. Such structure at an energy of approximately 531.5 eV has been attributed to surface defects or non-stoichiometric surface oxygen ions [44].

Conclusions

The application of XRD, XPS and FTIR spectroscopic methods in studying the effect of microwave radiation on the high phosphorus iron ore provides important information about the structure and oxidation state of the iron oxides. The results indicated that after microwave treatment the three different iron ore samples affected similarly.

XRD analysis showed that the peak intensity (crystallinity) of hematite increases after microwave treatment, but no phase change occurs. On the other hand, FTIR analysis showed that, after microwave radiation the functional chemical groups of phosphorus bearing minerals (fluoroapatite) and others gangues dissociated due to interaction of mineral matter with gangue.

High resolution XPS analyses of Fe 2p peaks, O 1s peaks, Fe 2p shake up satellite peaks and full wide at half maximum (FWHM) values for untreated and microwave treated samples showed that after microwave radiation a portion of Fe (+III) was reduced to Fe (+II). This means that after microwave radiation iron oxide (hematite, Fe^{3+}) transformed into more magnetic phase (Fe^{2+}). These results indicated that microwave radiation had a positive effect on the magnetic properties of iron oxide, through the formation of ferromagnetic phases. This improvement in magnetic properties will facilitate magnetic separation of iron bearing minerals from associated gangue minerals including phosphate.

Acknowledgments

The authors acknowledge CIMO (Center for International Mobility, Finland) and (Cultural Affair and Mission Sector, Egypt) for their financial grant for performing the present research work. The authors thank Mr. Riku Mattila and Mr. Tommi Kokkonen for their technical support throughout this work. The authors are indebted to Mr. Ari Väliheikki for help in FTIR analyses and Mr. Santtu Heinilehto for the XPS analyses.

References:

[1] G. Roussy, J.A. Pearce, Physical and Chemical Processes, Chapters 10, 11, 12, Wiley, 1995.

[2] K.E. Haque, Int. J. Miner. Process. 57 (1999) 1–24.

[3] D.A. Jones, T.P. Lelyveld, S.D. Mavrofidis, S.W. Kingman, N.J. Miles, Res., Cons. and Rec. 34 (2002) 75–90.

[4] M. Omran, T. Fabritius, A. M. Elmahdy, N. A. Abdel-Khalek, M. El-Aref, A. Elmanawi, Sep. Purif. Technol. 136 (2014) 223−232

[5] M. Omran, T. Fabritius, R. Mattila, Powder Technol. 269 (2015) 7–14.

[6] M. Omran, T. Fabritius, N. Abdel-Khalek, M. El-Aref, A.E.-H. Elmanawi, M. Nasr, A. Elmahdy, Journal of Minerals and Materials Characterization and Engineering, 2 (2014), 414-427.

[7] W. Zhao, J. Chen, X. Chang, S. Guo, C. Srinivasakannan, G. Chen, J. Peng, App. Surf. Sci. 300 (2014) 171-177.

[8] G. Chen, J. Chen, S. Guo, J. Li, C. Srinivasakannan, J. Peng, App. Surf. Sci. 258 (10) (2012) 4826-4829.

[9] G. Chen, J. Chen, J. Li, S. Guo, C. Srinivasakannan, J. Peng, Powd. Technol. 232 (2012) 58-63.

[10] G. Chen, J. Chen, Z. Y. Zhang, S. H. Guo, Z. B. Zhang, J. H. Peng, C. Srinivasakannan, X. Q. Li, Y. K. Zhuang, Z. M. Xu, Metallurgist, 57(7-8) (2013) 647-653.

[11] M. C. Biesinger, B. P. Payne, A. P. Grosvenor, L. W.M. Lau, A. R. Gerson, R. smart, App. Surf. Sci. 257 (2011) 2717–2730.

[12] N.S. McIntyre, D.G. Zetaruk, Anal. Chem. 49 (1977) 1521-1529.

[13] G. C. Allen, M. T. Curtis, A. J. Hooper, and P. M. Tucker, J. Chem. Soc., Dalton Trans., 14, (1974) 1525-1530.

[14] A. Mekki, D. Holland, C.F. McConville, M. Salim, J. Non-Cryst. Solids 208 (1996) 267-276.

[15] A.P. Grosvenor, B.A. Kobe, M.C. Biesinger, N.S. McIntyre, Surf. Interface Anal. 36 (2004) 1564-1574.

[16] R.P. Gupta, S.K. Sen, Phys Rev. B 12 (1975) 15-19.

[17] M.A. EL Sharkawi, M.M. EL Aref, A.A. Mesaed, Geol. Soc. Egypt, Spec. Publ. No. 2 (1996) 243-278.

[18] M.M. El Aref, M.A. EI Sharkawi, A.A. Mesaed, Geol. Soc. Egypt, Spec. Publ. No. 2 (1996) 279-312.

[19] K.E. Waters, N.A. Rowson, R.W. Greenwood, A.J. Williams, Sep. Purif. Technol. 46 (2007) 9–17.

[20] I. Florek, M. Lovas, I. Murova, Proceedings of the 31st Int. Microwave Power Symposium, 1996.

[21] K. Barani, S. M. J. Koleini, B. Rezaei, Sep. Purif. Technol. 76(3) (2011) 331-336.

[22] Gotic, M., Music, S., J. Mol. Struct. 834–836 (2007) 445–453.

[23] Iglesias, J.E., Serna, C.J., Mineral. Petrogr. Acta 29 (1985) 363–370.

[24] H. M. Baioumy, M. Z. Khedr, A. H. Ahmed, Ore Geol. Rev. 53 (2013) 63–76.

[25] Guo Chen, Zengkai Song, Jin Chen, Jinhui Peng, C. Srinivasakannan, J. Alloy. Comp. 577 (2013) 610–614.

[26] Guo Chen, Zengkai Song, Jin Chen, C. Srinivasakannan, Jinhui Peng, J. Alloy. Comp. 579 (2013) 612–616.

[27] M. L. Hair, J. Non-Cryst. Solids 19 (1975) 299–309.

[28] L. Verdonck, S. Hoste, F. F. Roelandt, G. P. Van der Kelen, J. Mol. Struct. 79 (1982) 273–279.

[29] H. D. Ruan, R. L. Forst, J. T. Kloprogge, Spectrochemica Acta Part A 57 (2001) 2575–2586.

[30] A. Dimirkoua, A. Ioannoub, M. Doulaa, Advan. Colloid and Interface Sci., 97 (2002) 37- 61.

[31] Michael E. Fleet, Xi Liu, J. Solid State Chem. 181 (2008) 2494– 2500

[32] S.J. Roosendaal, B. van Asselen, J.W. Elsenaar, A.M. Vredenberg, F.H.P.M. Habraken, Surf. Sci. 442 (1999) 329-337.

[33] P.C.J. Graat, M.A.J. Somers, Appl. Surf. Sci. 100 (1996) 36-40.

[34] P. Mills, J.L. Sullivan, J. Phys. D: Appl. Phys. 16 (1983) 723−732.

[35] D.D. Hawn, B.M. DeKoven, Surf. Interface Anal. 10 (1987) 63-74.

[36] M. Muhler, R. SchlÖgl, G. Ertl, J. Catal. 138 (1992) 413-444.

[37] C.D. Wagner, L.H. Gale, R.H. Raymond, Anal. Chem. 51 (1979) 466-482.

[38] A.G. Nasibulin, S. Rackauskas, H. Jiang, Y. Tian, P.R. Mudimela, S.D. Shandakov, L.I. Nasibulina, J. Sainio, E.I. Kauppinen, Nano Research 2 (2009) 373–379.

[39] M. Aronniemi, J. Sainio, J. Lahtinen, Surf. Sci. 578 (2005) 108–123.

[40] Lu Yuan, Yiqian Wang, Rongsheng Cai, Qike Jiang, Jianbo Wang, Boquan Li, Anju Sharma, Guangwen Zhou, Mater. Sci. Eng. B 177 (2012) 327 – 336.

[41] A. Barbieri, W. Weiss, M.A. Van Hove, G.A. Somorjai, Surf. Sci. 302 (1994)259−279.

[42] S. Jain, A.O. Adeyeye, S.Y. Chan, C.B. Boothroyd, J. Phys. D: Appl. Phys. 37 (2004) 2720−2725.

[43] K. Wandelt, Surf. Sci. Rep. 2 (1982)1-121.

[44] C. R. Brundle, T. J. Chuang, K. Wandelt, Surf. Sci. 68 (1977) 459-468.

[45] T. Fujii, F.M.F. de Groot, G.A. Sawatzky, F.C. Voogt, T. Hibma, K. Okada, Phys. Rev. B 59 (1999) 3195-3202.

[46] M. Aronniemi, J. Lahtinen, P. Hautojärvi, Surf. Interface Anal. 36 (2004) 1004–1006

[47] G. M. lngo, G. Padeletti, G. Chiozzini and G. Bultrini, J. Therm. Anal. 47 (1996) 263-272.

[48] G. M. Ingo, S. Mazzoni, G. Bltrini, S. Fntana, G, Padeletti, G. Chiozzini, L. Scoppio, Surf. Interface Anal. 22 (1994) 614-619.

[49] M. Descostes, F. Mercier, N. Thromat, C. Beaucaire, M. Gautier-Soyer, App. Surf. Sci. 165 (2000) 288–302.

[50] D.C. Frost, C. A. McDowell, J. S. Woolsey, Mol. Phys. 27 (1974) 1473-89.

[51] D.C. Frost, A. Ishitani, C.A. McDowell, Mol. Phys. 24(1972) 861-877.

[52] A. R. Pratt, I. J. Muir, H. W. Nesbitt, Geochimica et Cosmochimica Acta. 58 (1994) 827-841.

Figures captions:

Fig. (1) X – ray diffraction pattern for iron ore samples. He = hematite, Go = goethite, P = fluorapatite, Q = quartz, and Ch = chamosite.

Fig. (2) SEM images of iron ores samples. Sample G3 , (A) SEM image shows the occurrence of hematite (He) as oolitic, (B) Enlargement of squared area in (A), (C) and (D) EDX analysis of the square areas (i) and (ii) in (B). Sample G2, (E) SEM image shows that sample composed mainly from oolitic hematite (He) and detrital quartz (Qz), with minor chamosite (Ch). Sample G1, (F) SEM image shows sample occur as fine-grained cement-like materials of hematite and phosphorus (P), (H) EDX analyses of the squared area in (F).

Fig. (3) TG-DSC curves (a), and (MS) mass spectrometry (b) for sample G1.

Fig. (4) TG-DSC curves (a), and (MS) mass spectrometry (b) for sample G2.

Fig. (5) TG-DSC curves (a), and (MS) mass spectrometry (b) for sample G3.

Fig. (6) XRD patterns for the untreated iron ore and for the iron ore after exposure to 900 W of microwave power for 60 s and 120 s exposure times (sample G1). He= hematite, Go= goethite, P= fluorapatite, Q= quartz, Ch= chamosite, and M= maghemite or magnetite.

Fig. (7) XRD patterns for the untreated iron ore and for the iron ore after exposure to 900 W of microwave power for 60 s and 120 s exposure times (sample G2). He= hematite, P= fluorapatite, Q= quartz, Ch= chamosite, and M= maghemite or magnetite.

Fig. (8) XRD patterns for the untreated iron ore and for the iron ore after exposure to 900 W of microwave power for 60 s and 120 s exposure times (sample G3). He= hematite, P= fluorapatite, Q= quartz, Ch= chamosite, and M= maghemite or magnetite.

Fig. (9) BSE images of microwave treated iron ore, indicating that melting occurred at the grain boundaries of the minerals. (A) and (B) BSE images of sample G3, (B) Enlargement of squared area in (A). (C) and (D) BSE images of sample G1, (D) Enlargement of squared area in (C). (E) and (F) BSE images of sample G2.

Fig. (10) FTIR spectra for sample G1; (a) untreated, (b) microwave treated iron ore for 60 s, and (c) microwave treated iron ore for 120 s

Fig. (11) FTIR spectra for sample G2; (a) untreated, (b) microwave treated iron ore for 60 s, and (c) microwave treated iron ore for 120 s

Fig. (12) FTIR spectra for sample G3; (a) untreated, (b) microwave treated iron ore for 60 s, and (c) microwave treated iron ore for 120 s

Fig. (13) Survey scan XPS spectra for sample G1; (a) untreated, (b) microwave treated iron ore for 120 s.

Fig. (14) Survey scan XPS spectra for sample G2; (a) untreated, (b) microwave treated iron ore for 120 s.

Fig. (15) Survey scan XPS spectra for sample G3; (a) untreated, (b) microwave treated iron ore for 120 s.

Fig. (16) Detail XPS spectra of Fe 2p and Fitted Fe $2p_{3/2}$ spectra for sample G1; (a) untreated, (b) microwave treated iron ore for 120 s.

Fig. (17) Detail XPS spectra of Fe 2p and Fitted Fe $2p_{3/2}$ spectra for sample G2; (a) untreated, (b) microwave treated iron ore for 120 s.

Fig. (18) Detail XPS spectra of Fe 2p and Fitted Fe $2p_{3/2}$ spectra for sample G3; (a) untreated, (b) microwave treated iron ore for 120 s.

Fig. (19) Detail and Deconvoluted XPS spectra of O 1s for sample G1; (a) untreated, (b) microwave treated iron ore for 120 s.

Fig. (20) Detail and Deconvoluted XPS spectra of O 1s for sample G2; (a) untreated, (b) microwave treated iron ore for 120 s.

Fig. (21) Detail and Deconvoluted XPS spectra of O 1s for sample G3; (a) untreated, (b) microwave treated iron ore for 120 s.

Table (1) Chemical analysis of the representative samples

Sample	FeO (%)	TFe (%)	P_2O_5 (%)	CaO (%)	F (%)	SiO_2 (%)	Al_2O_3 (%)	MgO (%)	MnO (%)
G1	62,18	48,33	5,64	7,59	0,37	15,03	3,37	1,23	1,76
G2	59,28	46,08	2,25	2,67	0,32	29,54	3,27	0,27	0,02
G3	74,96	58,27	3,24	5,44	0,19	7,48	4,47	1,26	0,54

Table (2) Matrix for microwave tests (900 W, 2.45 GHz).

Exposure time (s)	Sample temperature (°C)		
	Sample G1	Sample G2	Sample G3
60 s	490	516	546
120 s	778	794	828

Table

Figure 1

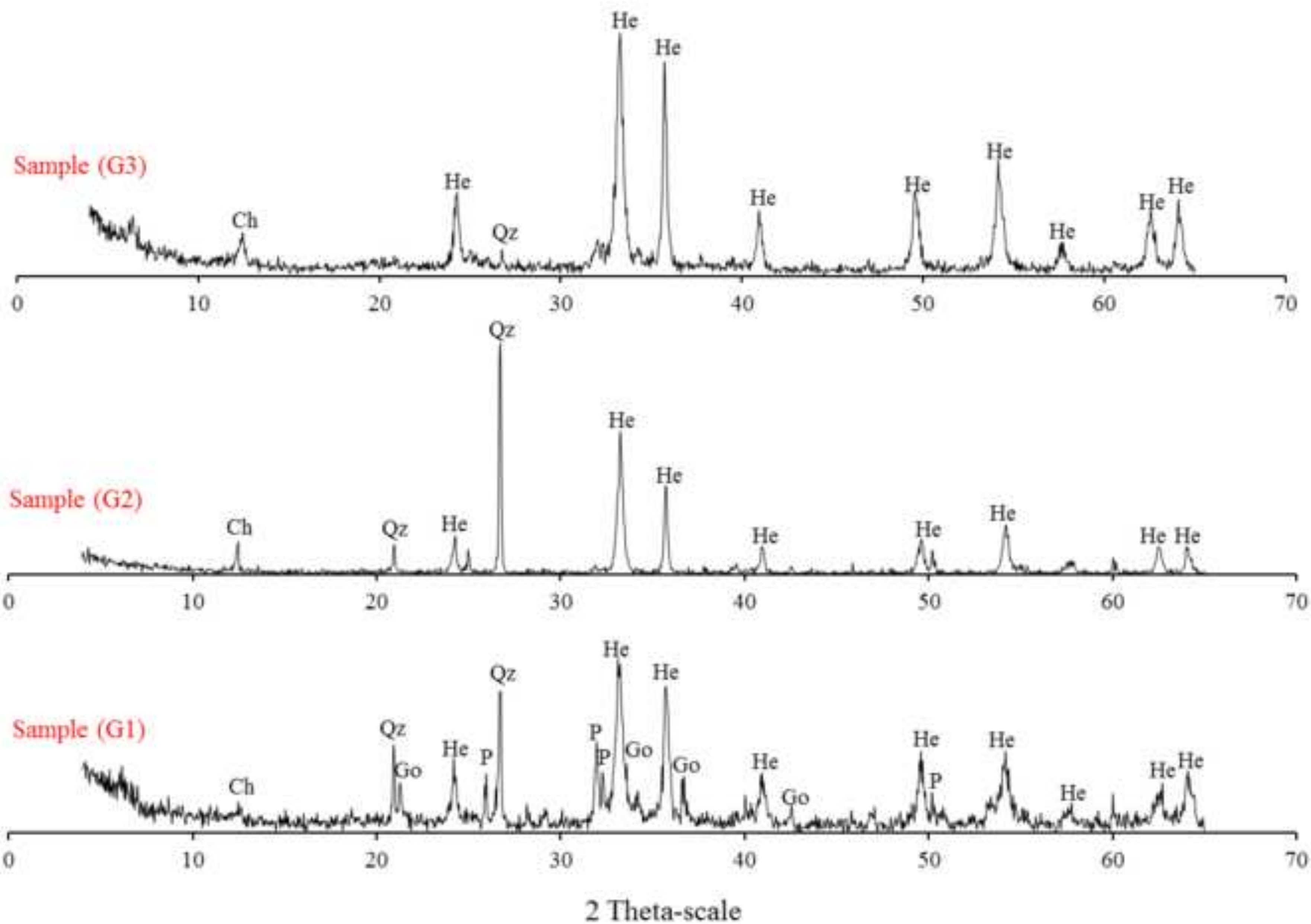

Table

Figure 2

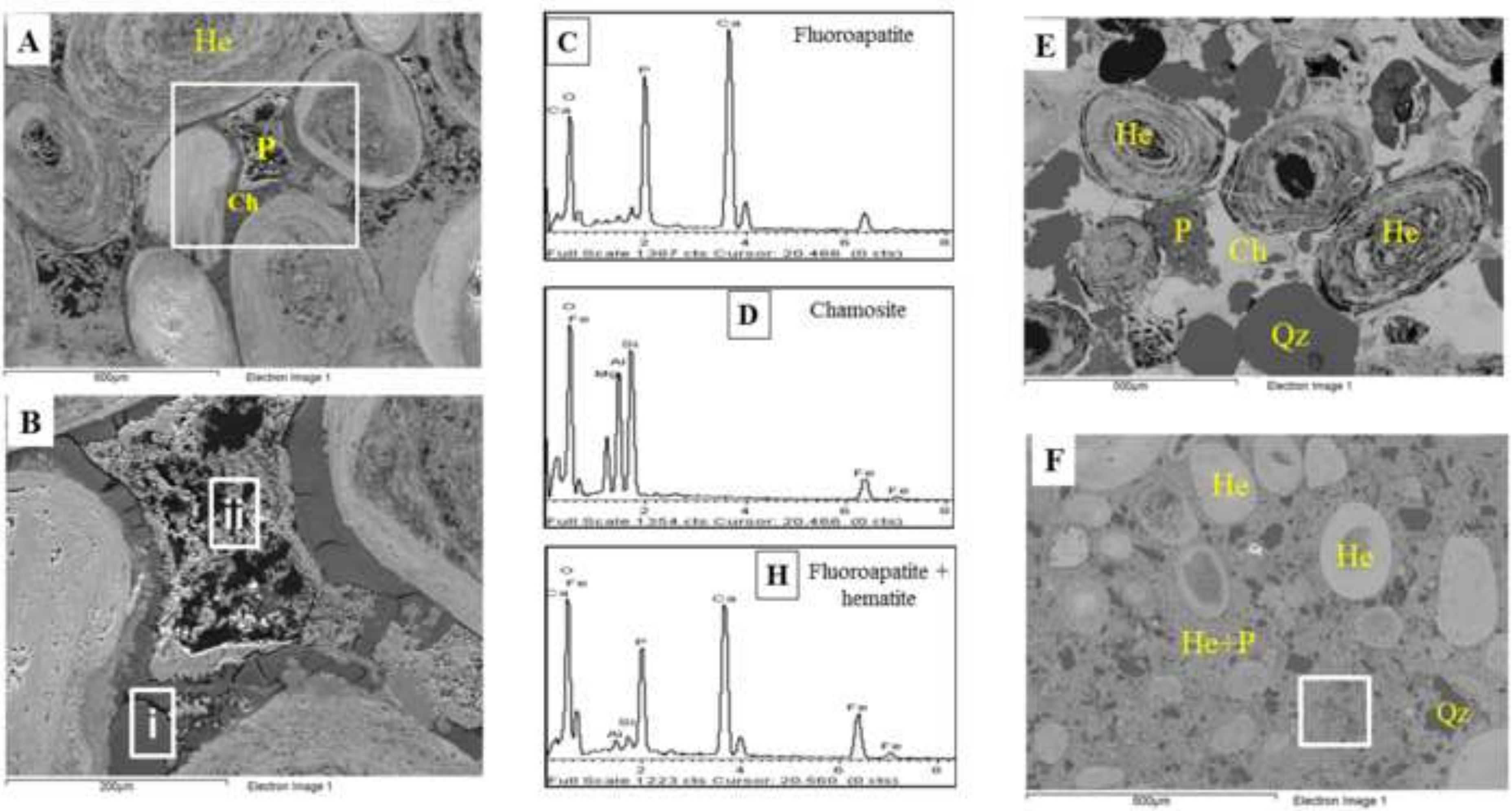

Figure 3

(a)

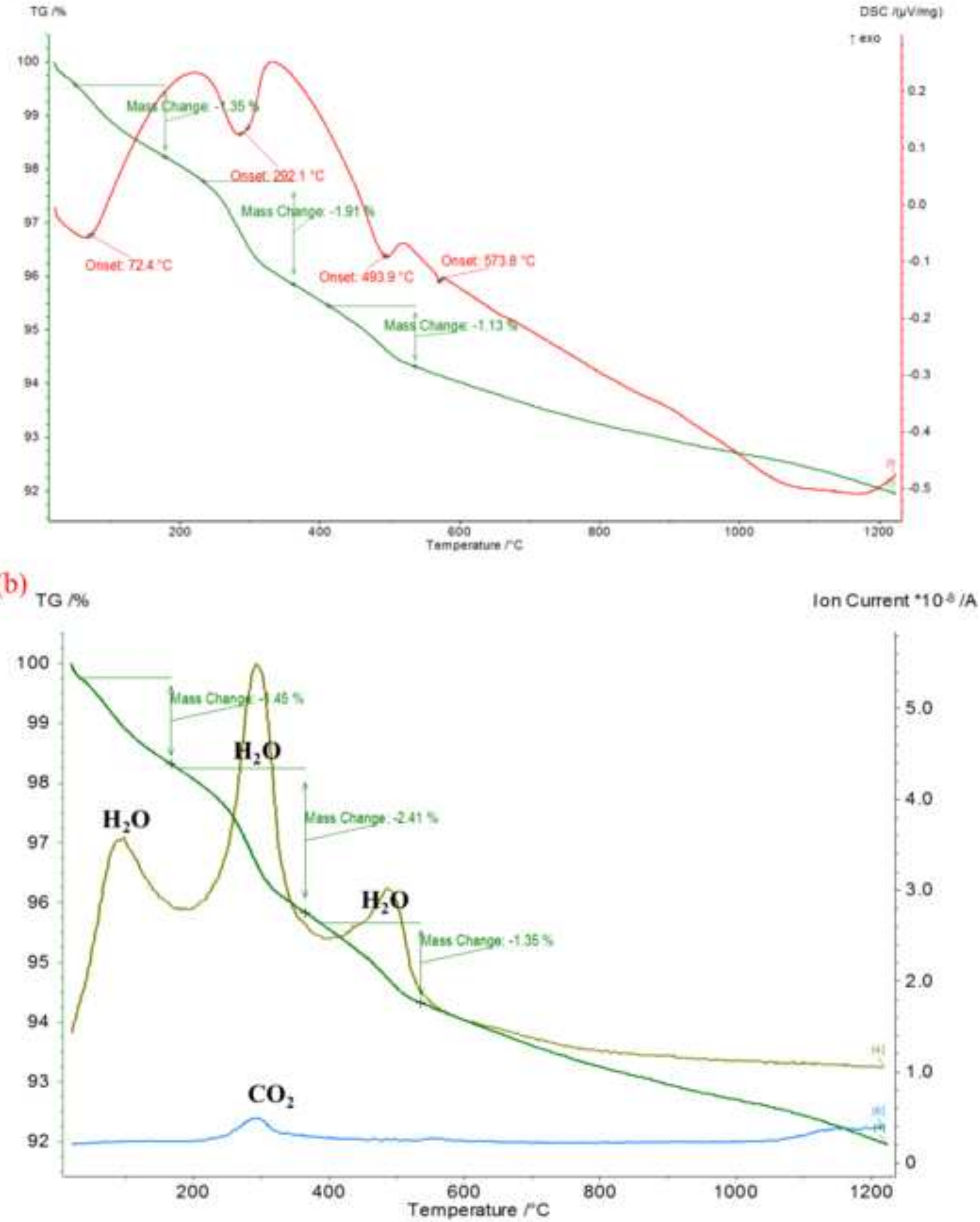

TG /%
DSC /(μV/mg)
↑ exo
Mass Change: -1.35 %
Mass Change: -1.91 %
Mass Change: -1.13 %
Onset: 72.4 °C
Onset: 292.1 °C
Onset: 493.9 °C
Onset: 573.8 °C
Temperature /°C
(b)
TG /%
Ion Current *10-8 /A
Mass Change: -1.45 %
Mass Change: -2.41 %
Mass Change: -1.35 %
H_2O
H_2O
H_2O
CO_2
Temperature /°C

Figure 4

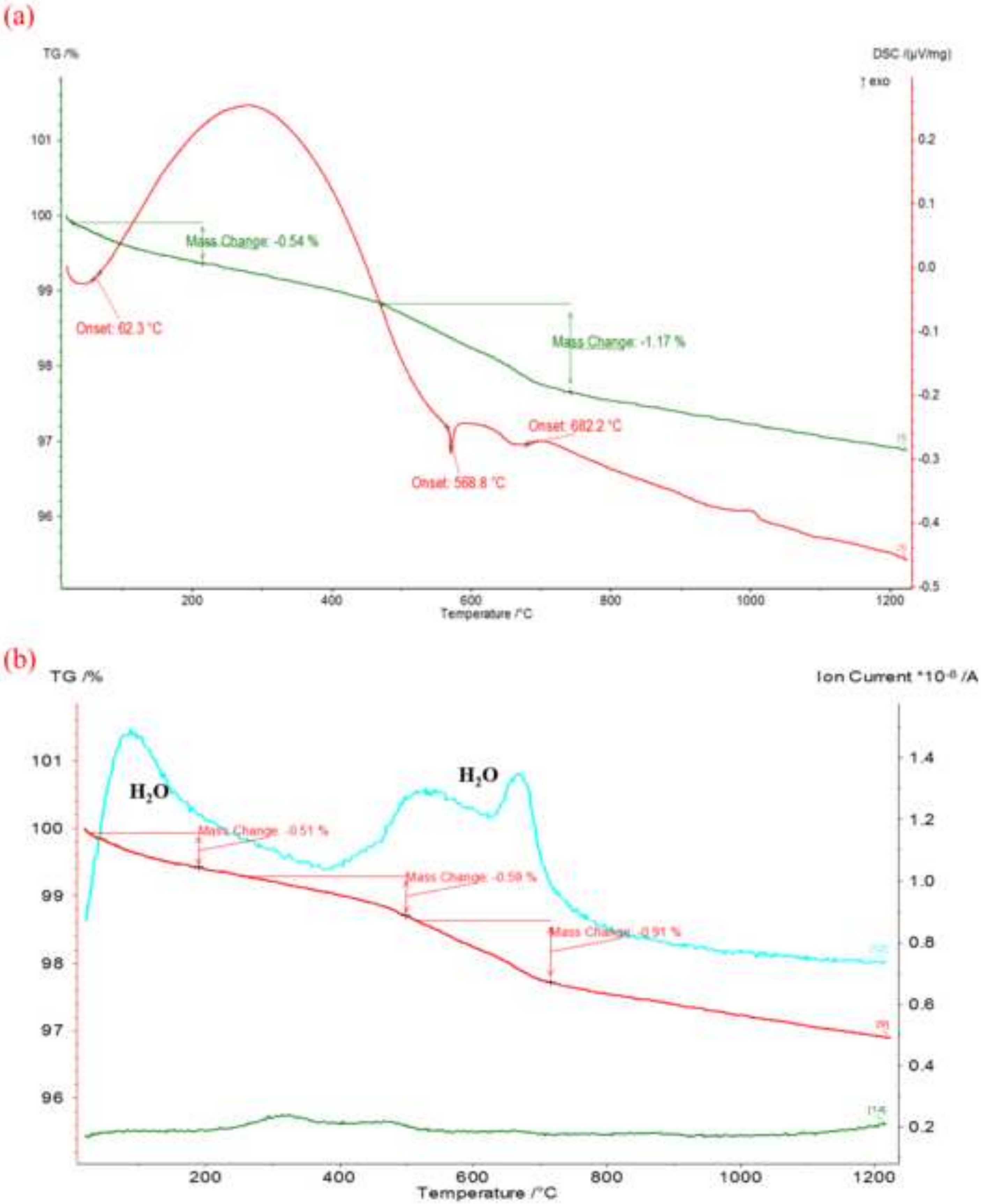
(a)
TG /%
DSC /(µV/mg)
↑ exo
Mass Change: -0.54 %
Mass Change: -1.17 %
Onset: 62.3 °C
Onset: 682.2 °C
Onset: 568.8 °C
Temperature /°C
(b)
TG /%
Ion Current *10-8 /A
H_2O
H_2O
Mass Change: -0.51 %
Mass Change: -0.59 %
Mass Change: -0.91 %
Temperature /°C

Figure 5

(a)

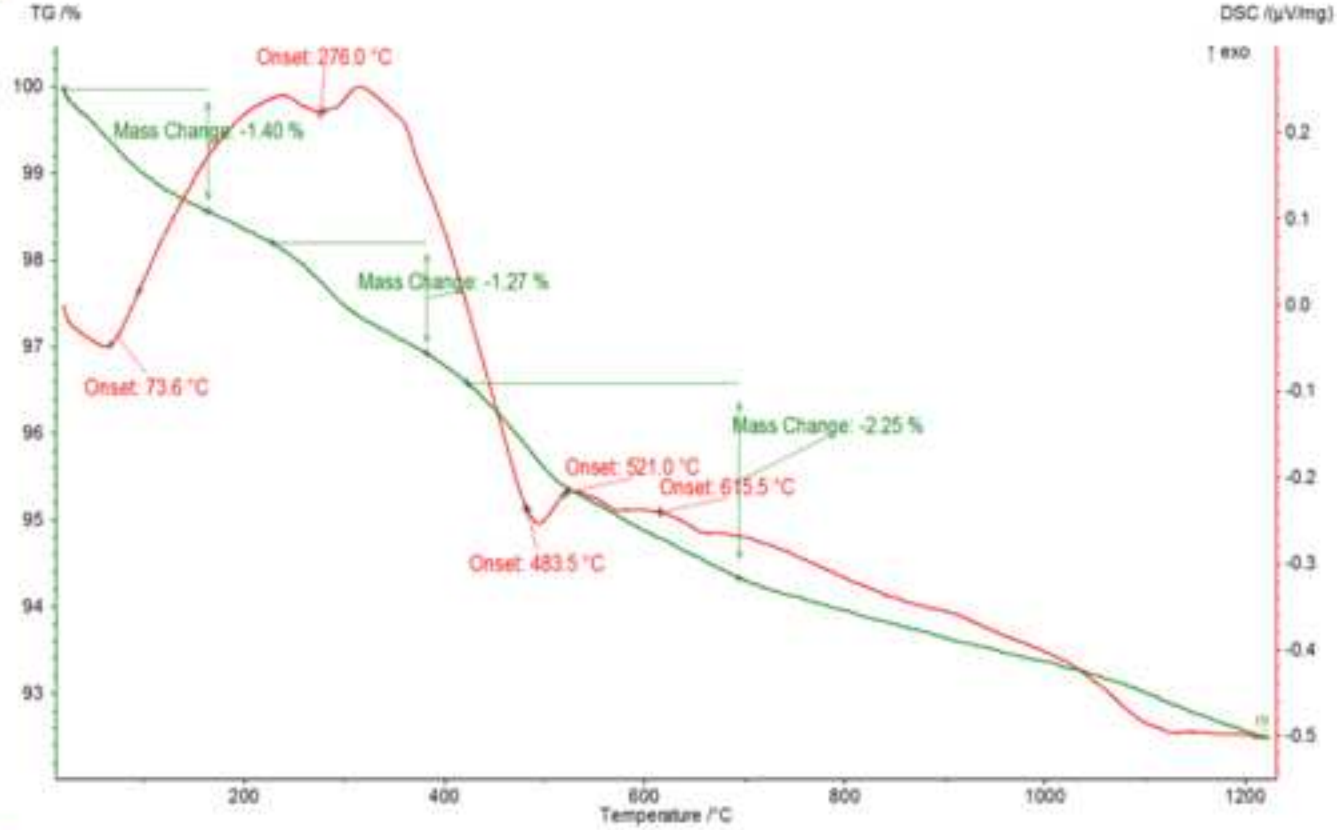
TG /%
DSC /(µV/mg)
↑ exo
Onset: 276.0 °C
Mass Change: -1.40 %
Mass Change: -1.27 %
Onset: 73.6 °C
Mass Change: -2.25 %
Onset: 521.0 °C
Onset: 615.5 °C
Onset: 483.5 °C
Temperature /°C

(b)

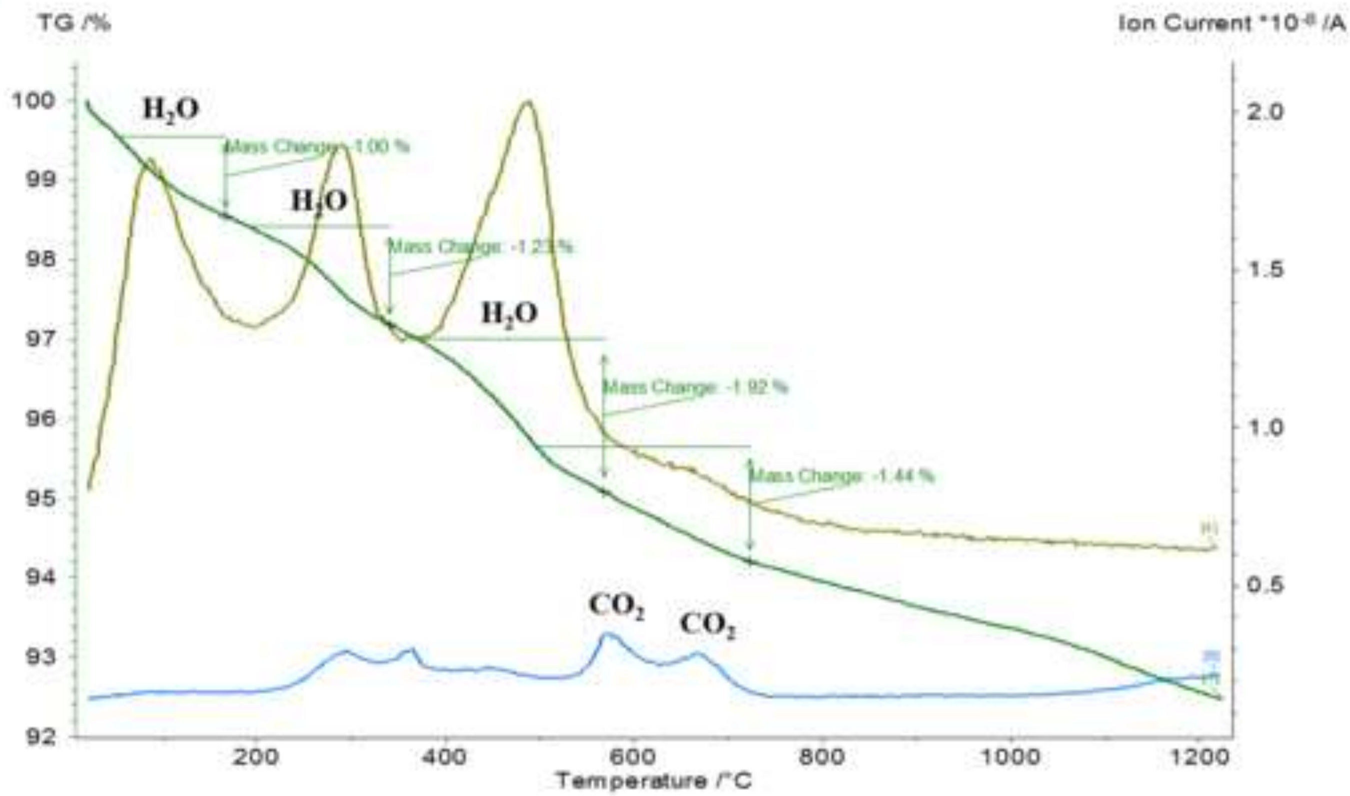
TG /%
Ion Current *10-8 /A
H2O
Mass Change: -1.00 %
H2O
Mass Change: -1.23 %
H2O
Mass Change: -1.92 %
Mass Change: -1.44 %
CO2
CO2
Temperature /°C

Table

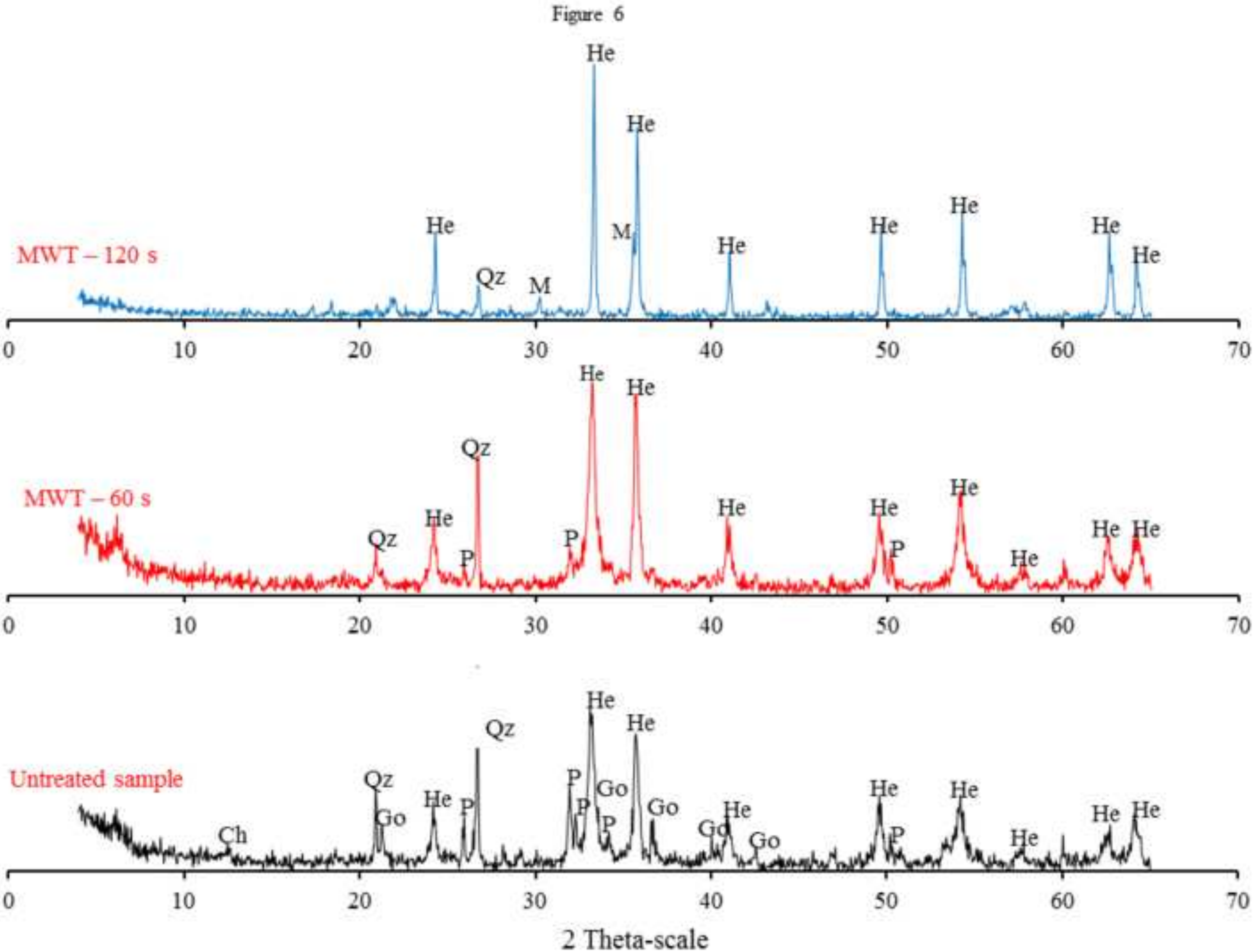

Figure 6
MWT – 120 s
MWT – 60 s
Untreated sample
He
Qz
M
P
Go
Ch
0
10
20
30
40
50
60
70
2 Theta-scale

Table

Figure 7

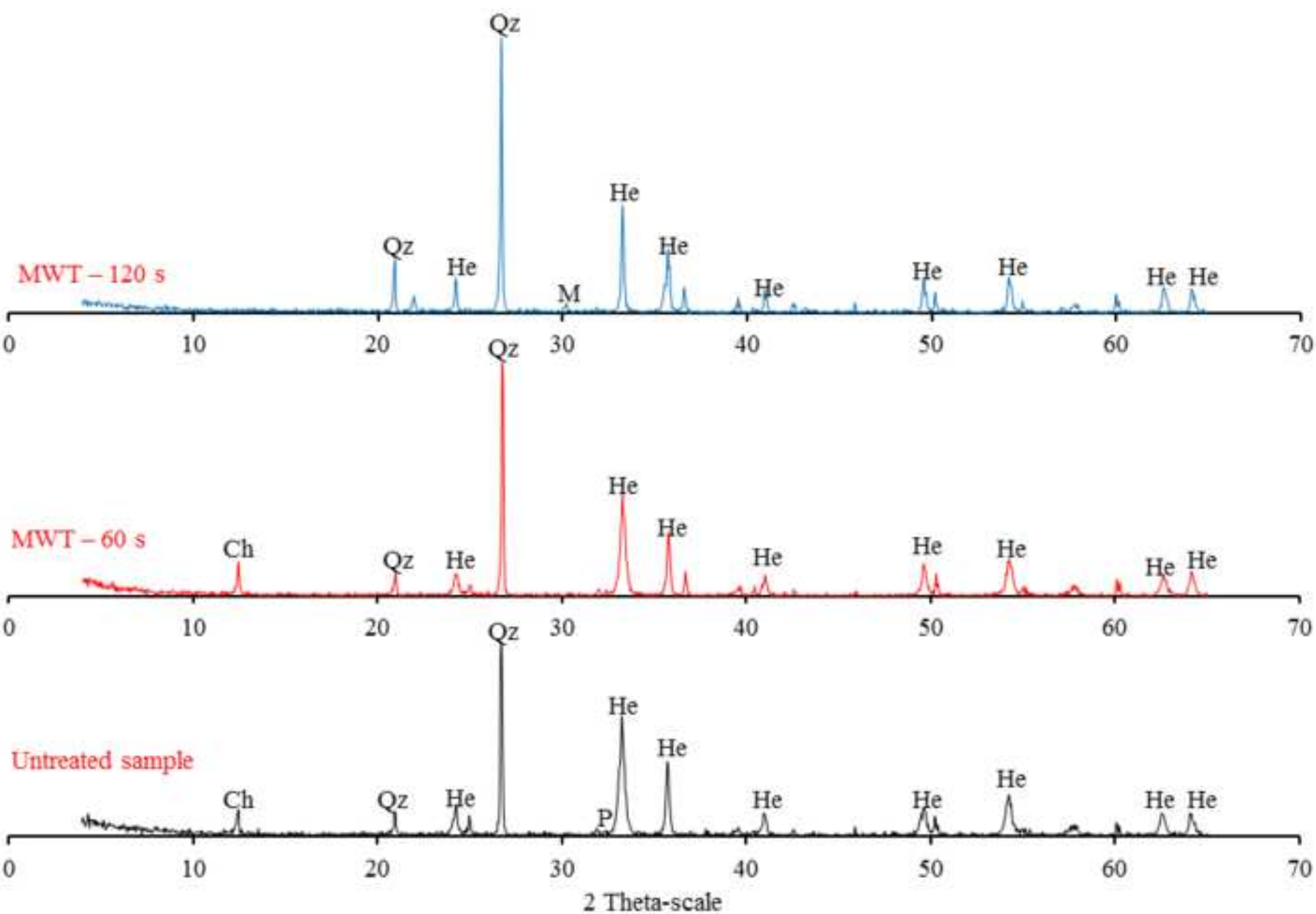

Table

Figure 8

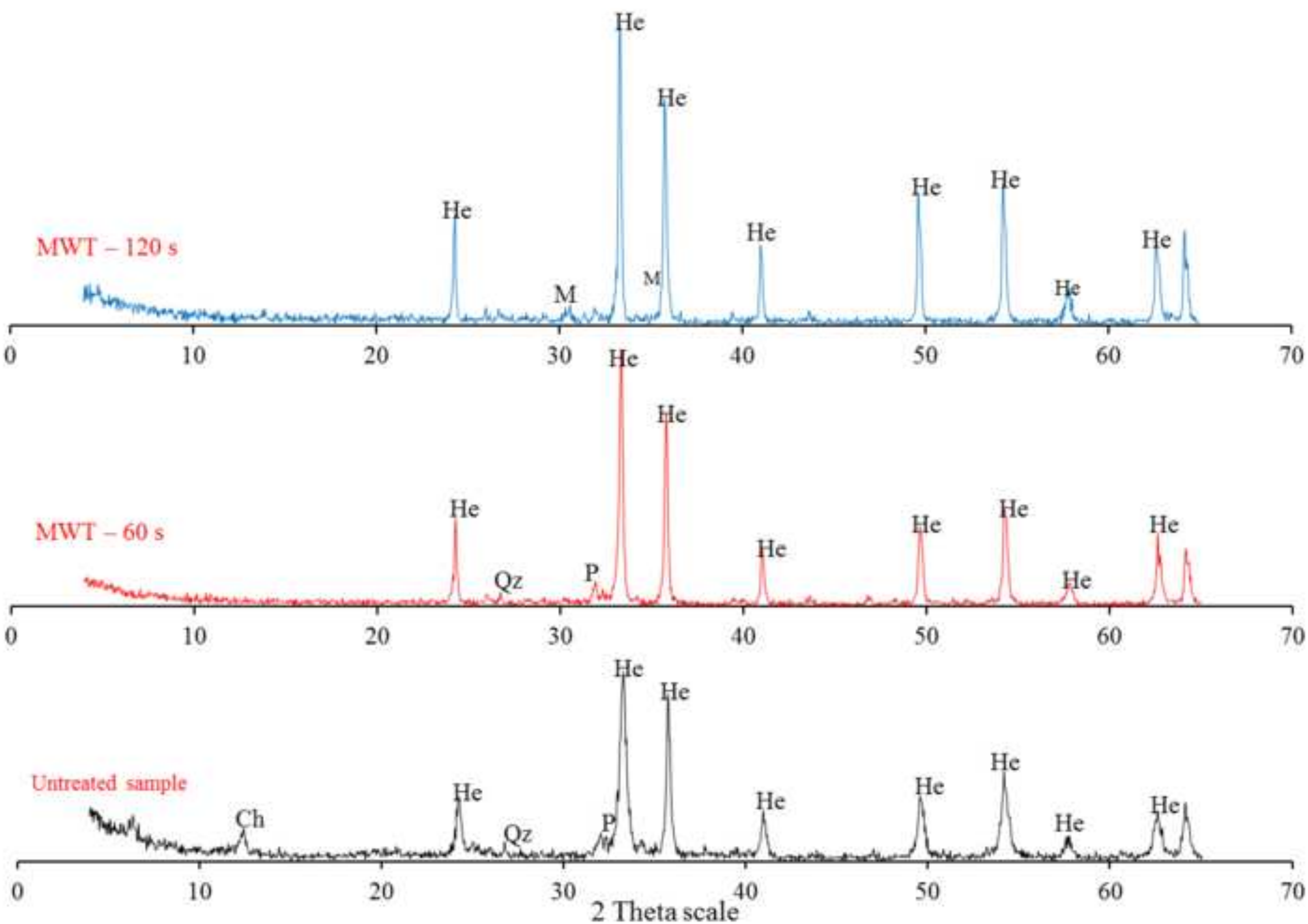

Figure 9

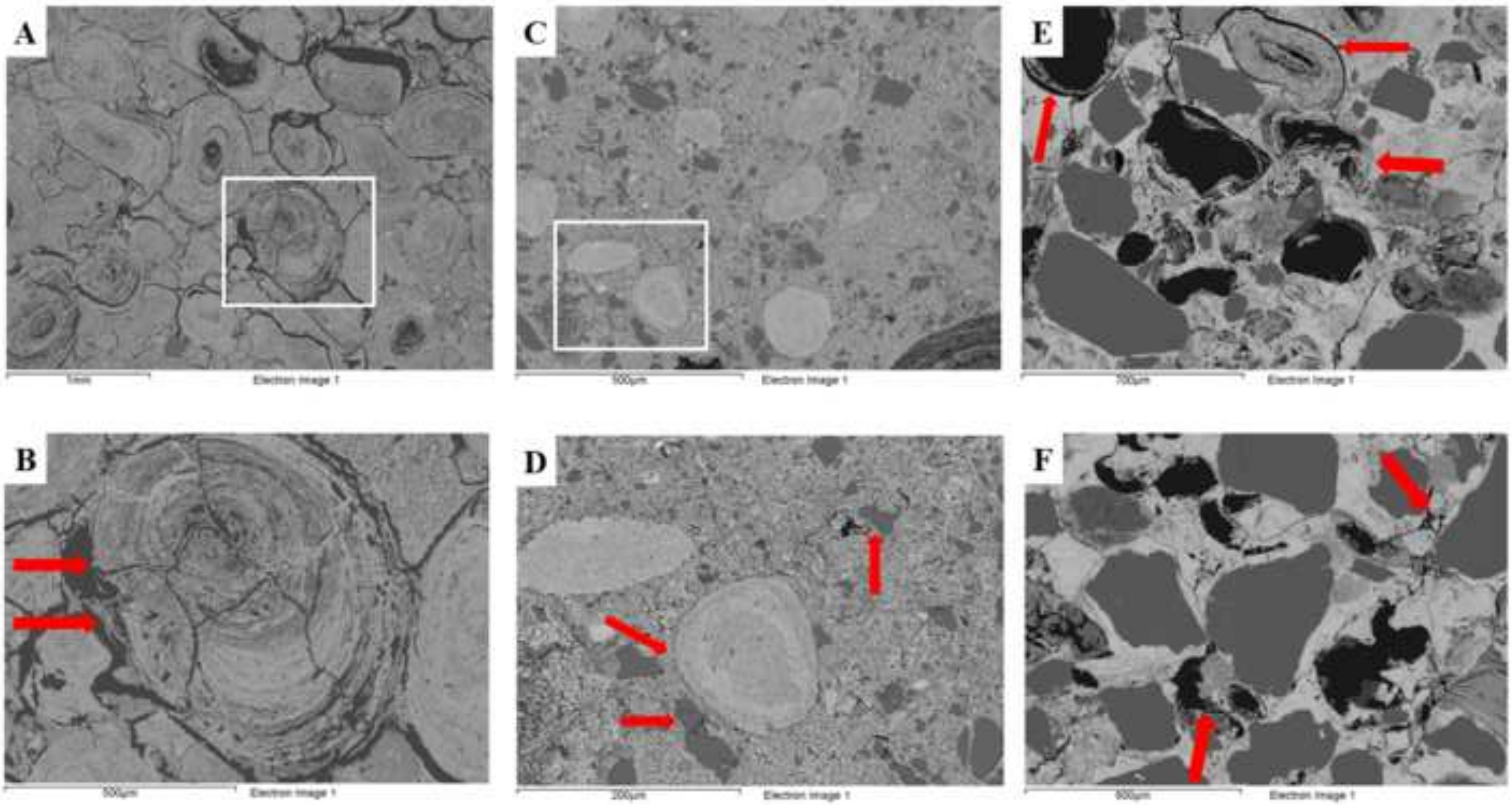

Table

Figure 10

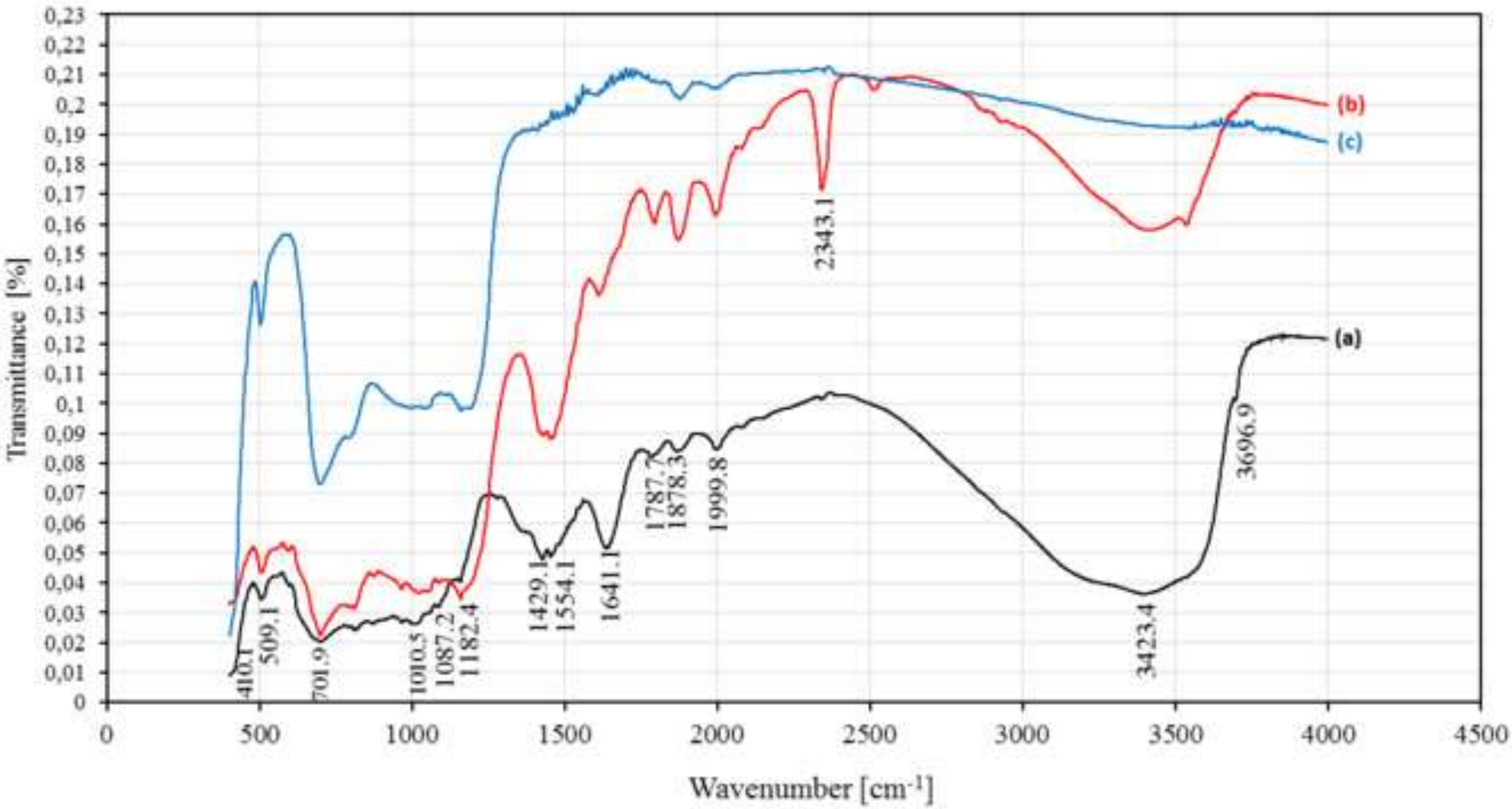

Table

Figure 11

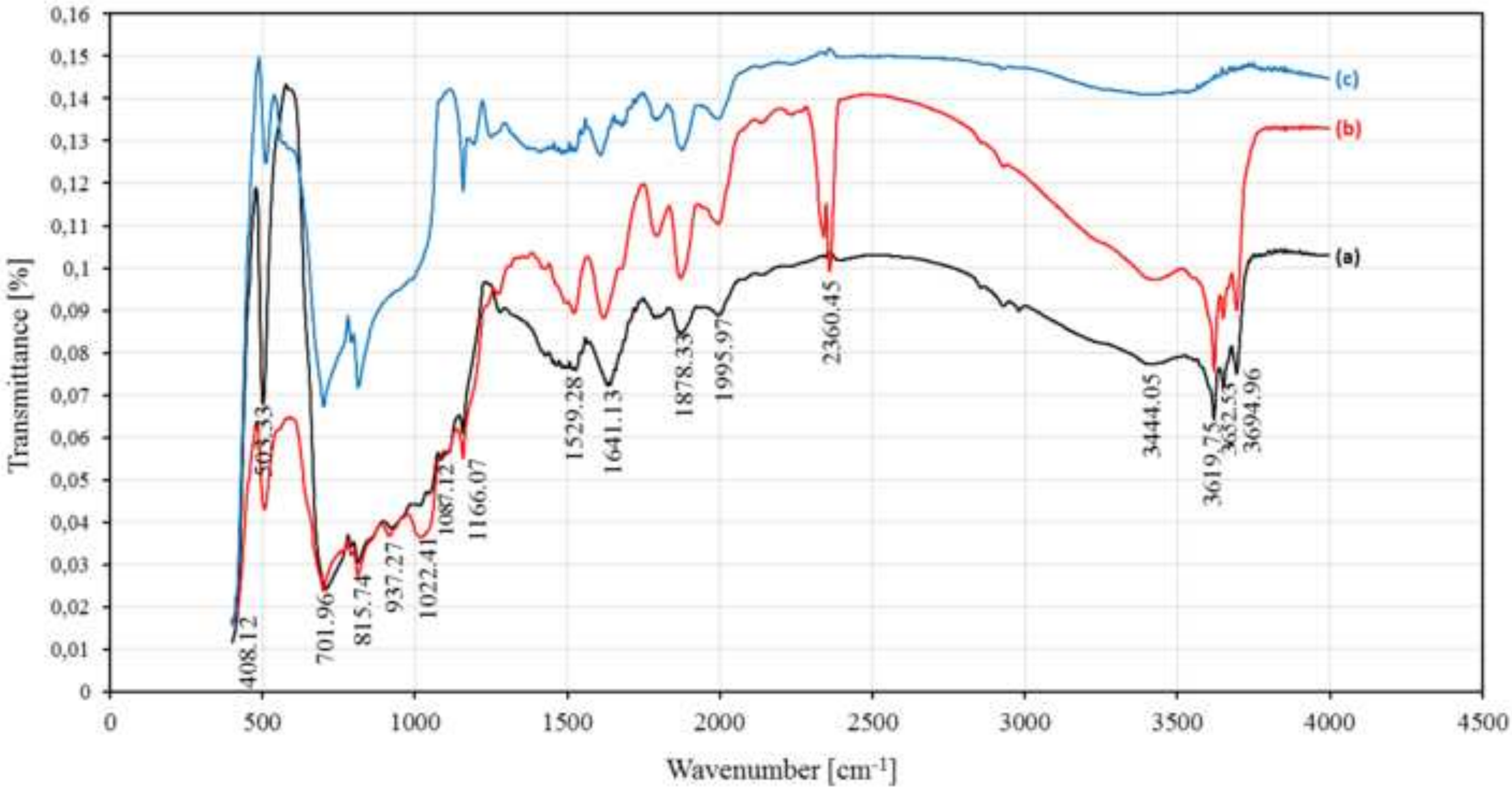

Table

Figure 12

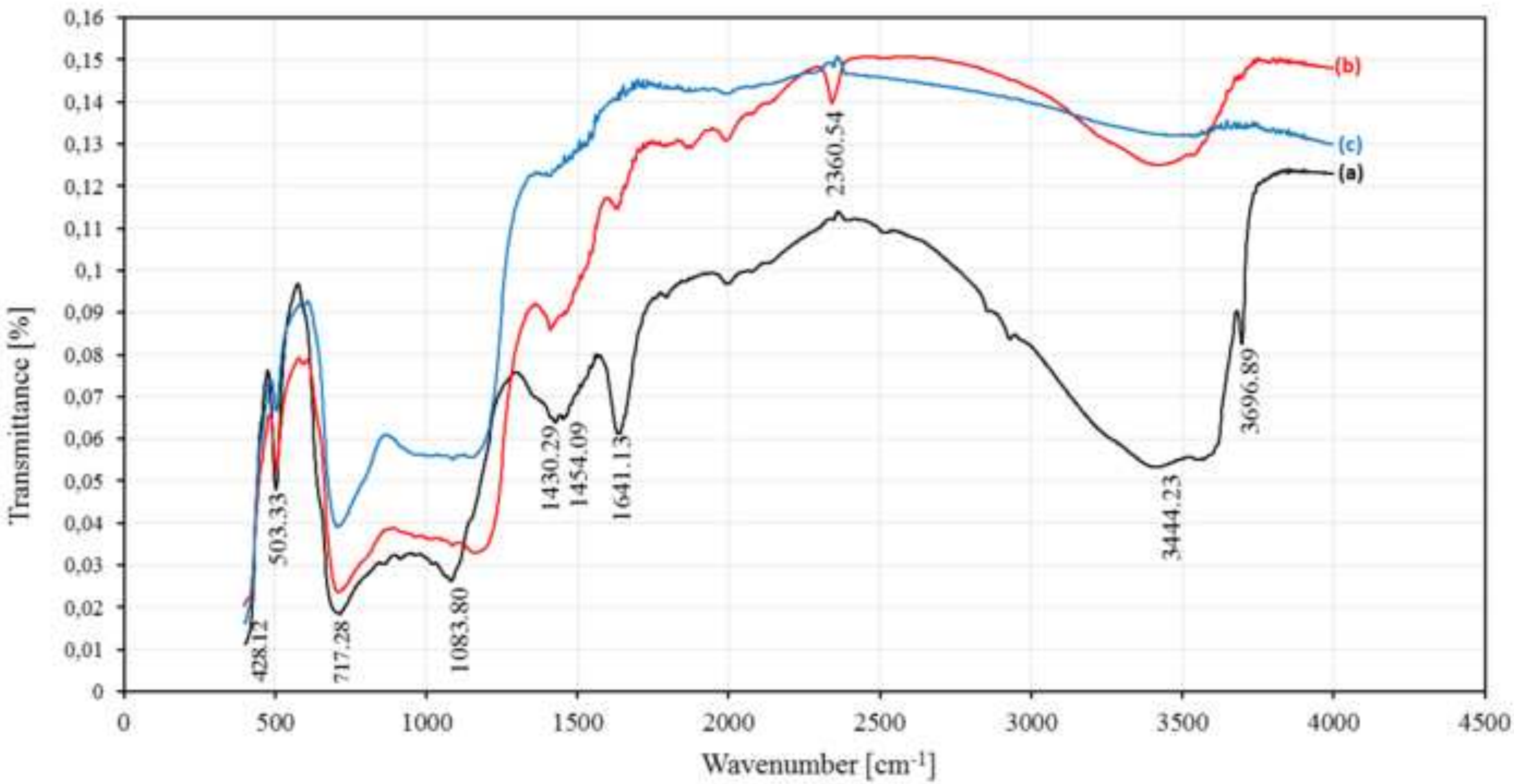

Figure 13

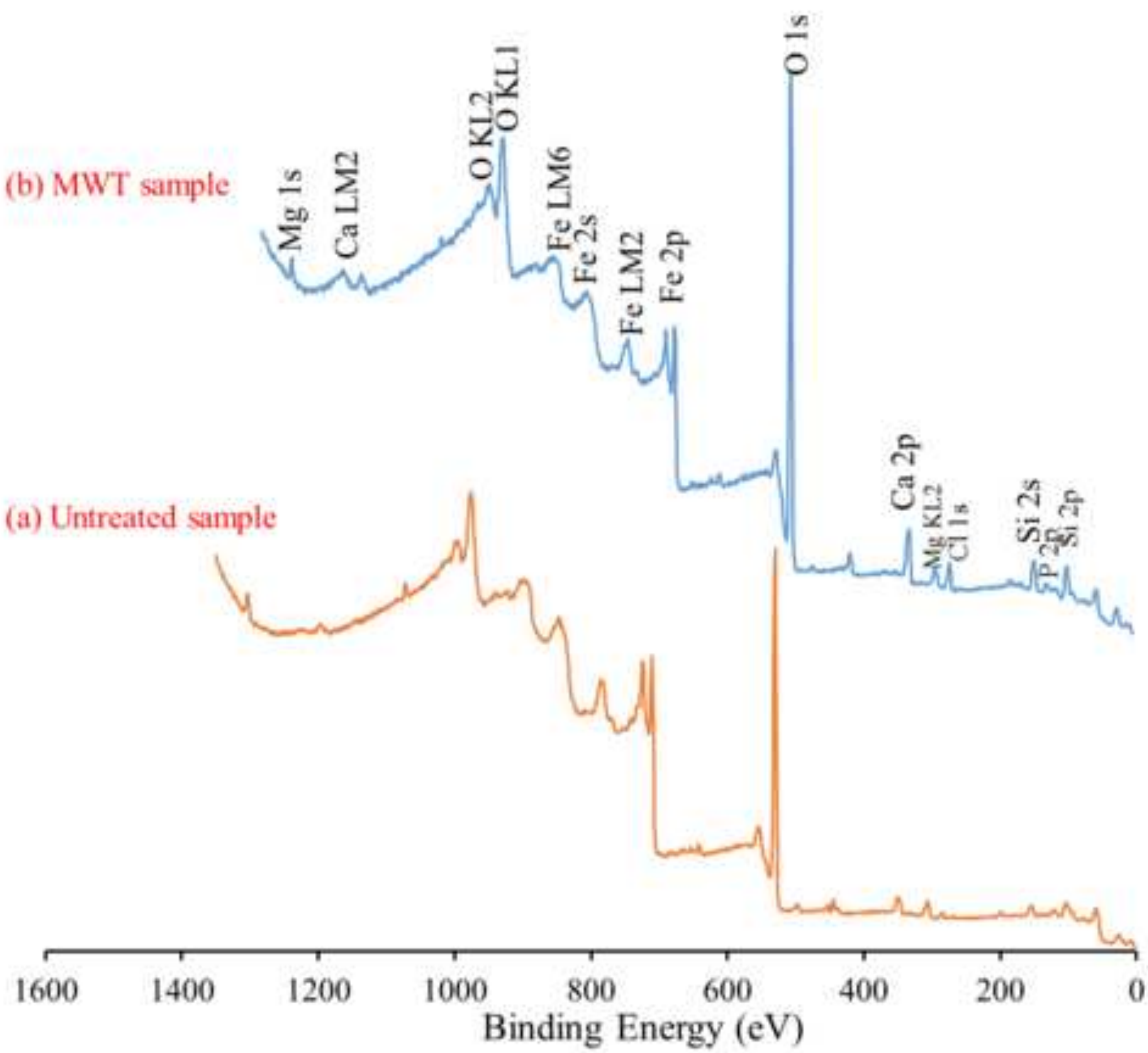
(b) MWT sample
(a) Untreated sample
Mg 1s
Ca LM2
O KL2
O KL1
Fe LM6
Fe 2s
Fe LM2
Fe 2p
O 1s
Ca 2p
Mg KL2
Cl 1s
Si 2s
P 2p
Si 2p
1600
1400
1200
1000
800
600
400
200
0
Binding Energy (eV)

Figure 14

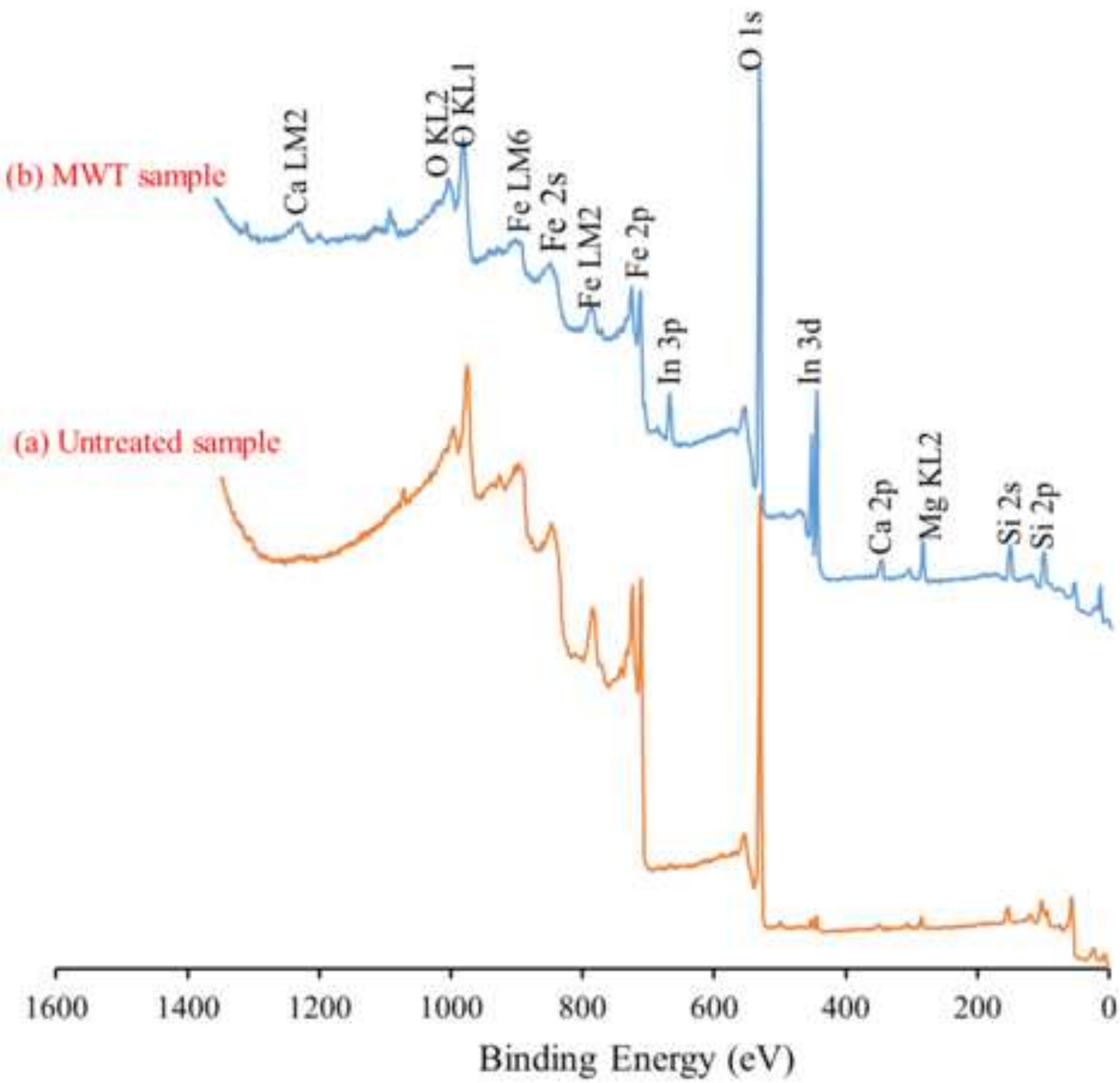
(b) MWT sample
(a) Untreated sample
Ca LM2
O KL2
O KL1
Fe LM6
Fe 2s
Fe LM2
Fe 2p
In 3p
O 1s
In 3d
Ca 2p
Mg KL2
Si 2s
Si 2p
1600
1400
1200
1000
800
600
400
200
0
Binding Energy (eV)

Figure 15

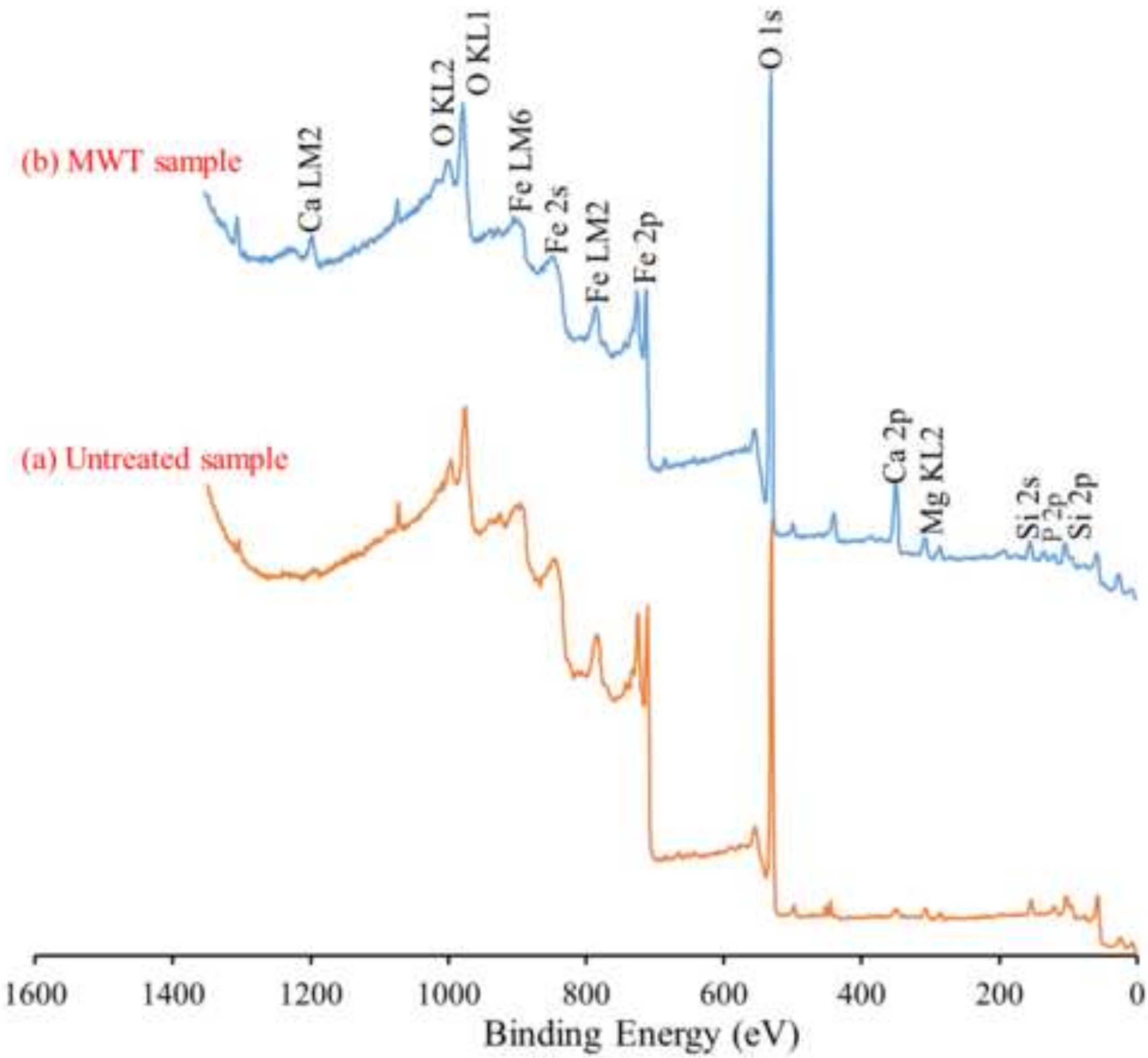
(b) MWT sample
(a) Untreated sample
Ca LM2
O KL2
O KL1
Fe LM6
Fe 2s
Fe LM2
Fe 2p
O 1s
Ca 2p
Mg KL2
Si 2s
P 2p
Si 2p
1600
1400
1200
1000
800
600
400
200
0
Binding Energy (eV)

Figure 16

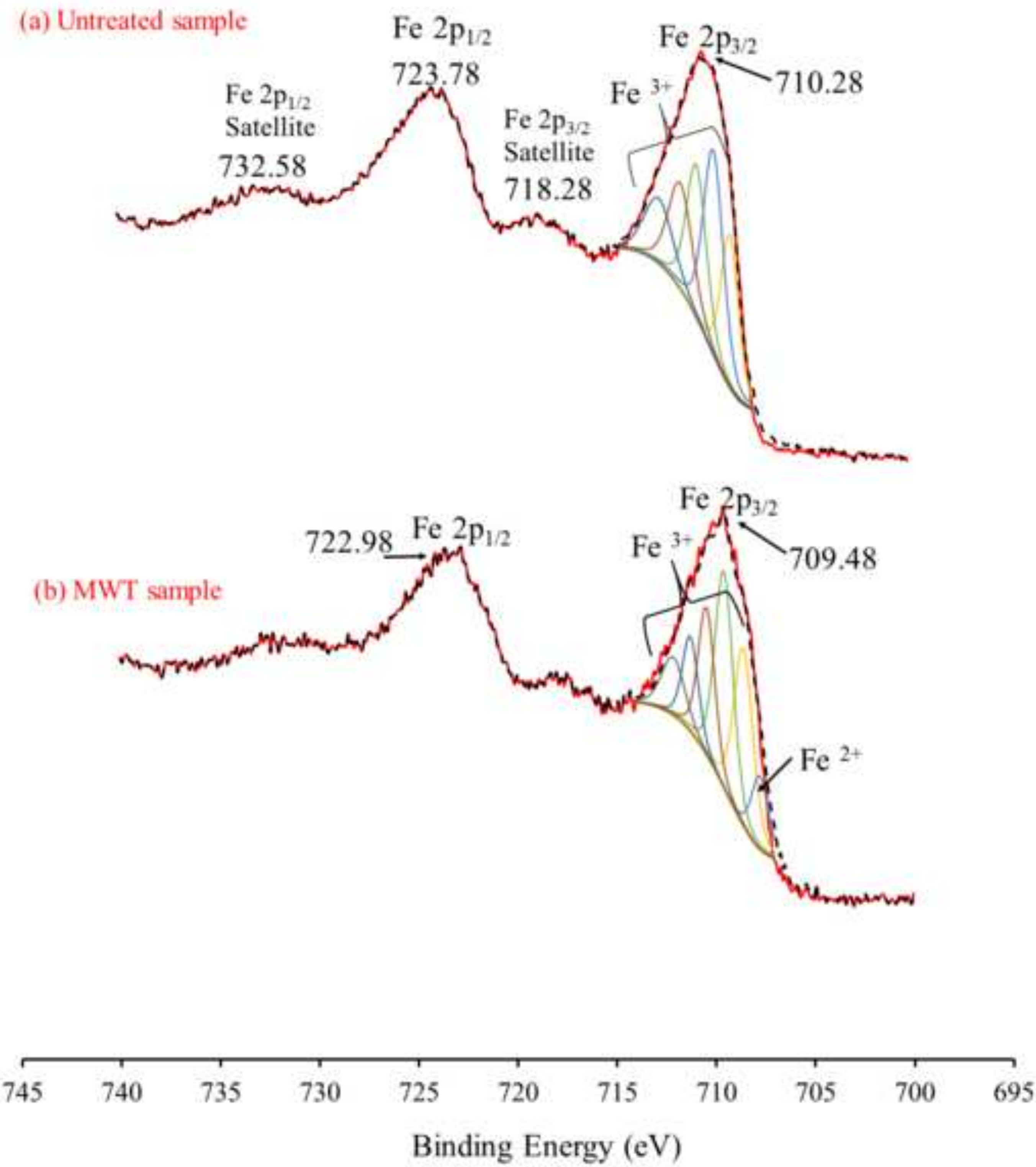
(a) Untreated sample
Fe 2p1/2
723.78
Fe 2p3/2
710.28
Fe 3+
Fe 2p1/2
Satellite
732.58
Fe 2p3/2
Satellite
718.28
Fe 2p3/2
722.98
Fe 2p1/2
Fe 3+
709.48
(b) MWT sample
Fe 2+
745
740
735
730
725
720
715
710
705
700
695
Binding Energy (eV)

Figure 17

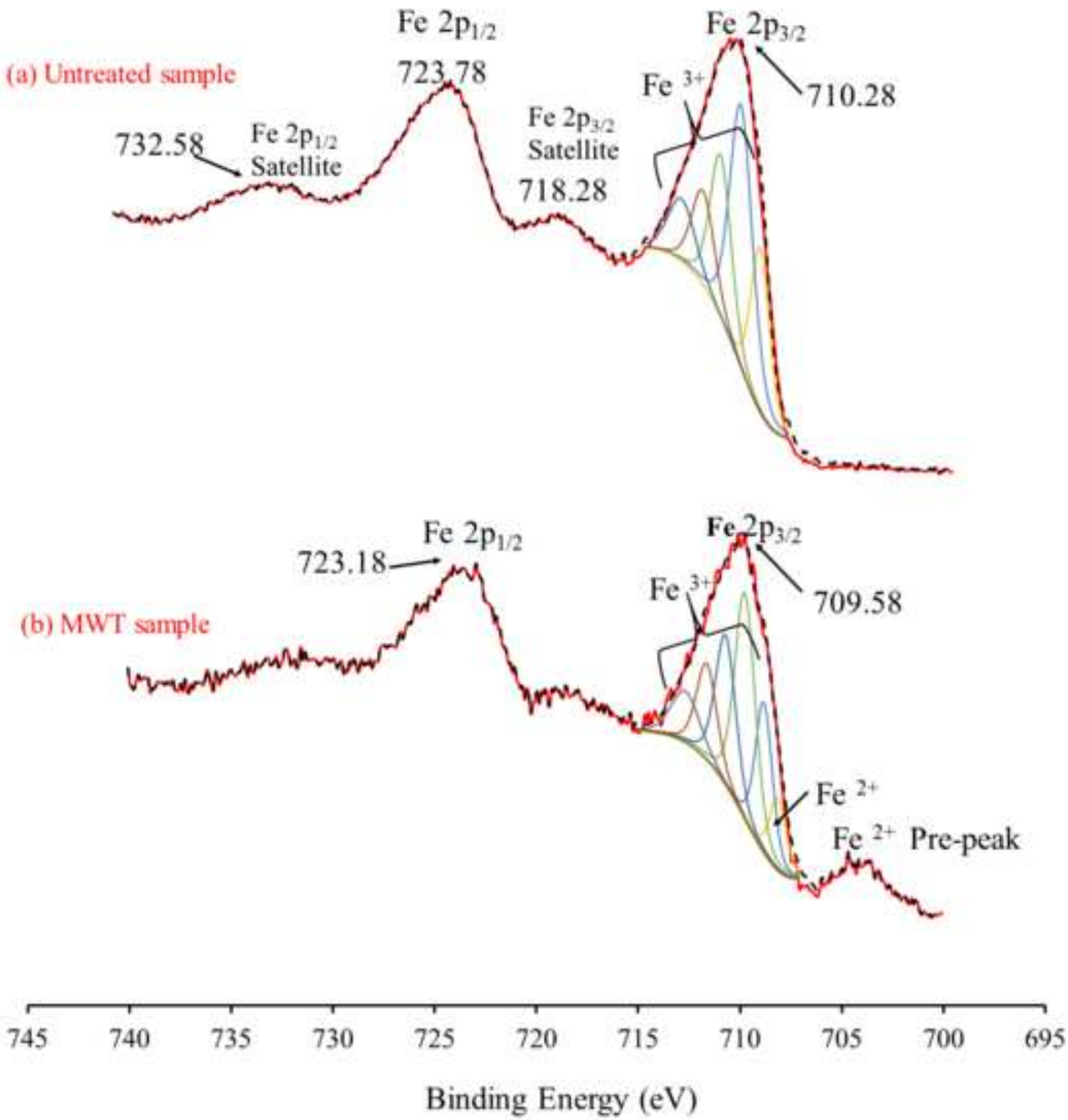

(a) Untreated sample
Fe 2p1/2
723.78
Fe 2p3/2
710.28
Fe 3+
732.58
Fe 2p1/2
Satellite
Fe 2p3/2
Satellite
718.28
(b) MWT sample
723.18
Fe 2p1/2
Fe 2p3/2
709.58
Fe 3+
Fe 2+
Fe 2+ Pre-peak
745
740
735
730
725
720
715
710
705
700
695
Binding Energy (eV)

Figure 18

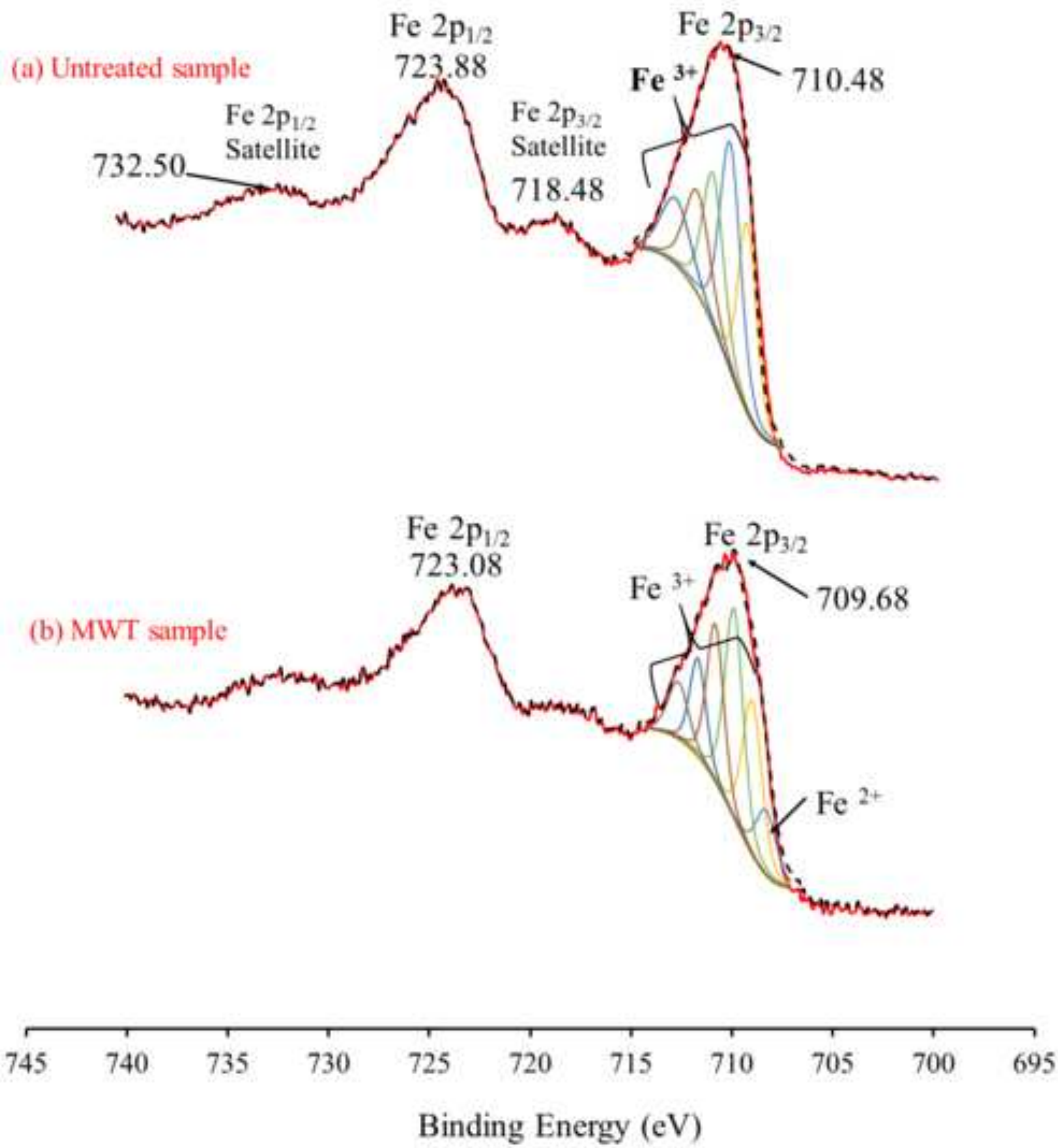

(a) Untreated sample
Fe 2p1/2
723.88
Fe 2p3/2
Fe 3+
710.48
Fe 2p1/2
Satellite
732.50
Fe 2p3/2
Satellite
718.48
(b) MWT sample
Fe 2p1/2
723.08
Fe 2p3/2
Fe 3+
709.68
Fe 2+
745
740
735
730
725
720
715
710
705
700
695
Binding Energy (eV)

Figure 19

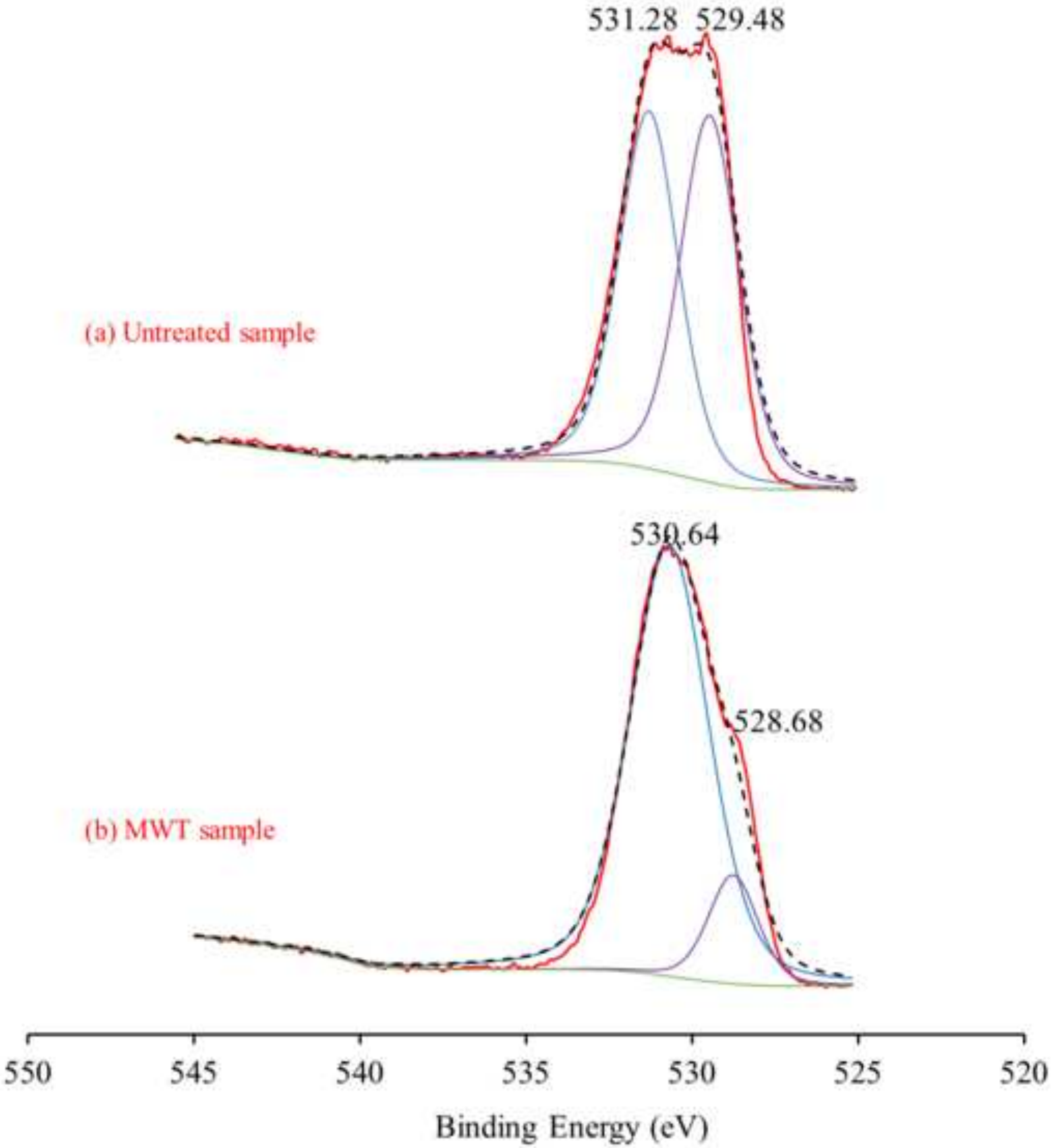
531.28
529.48
(a) Untreated sample
530.64
528.68
(b) MWT sample
550
545
540
535
530
525
520
Binding Energy (eV)

Figure 20

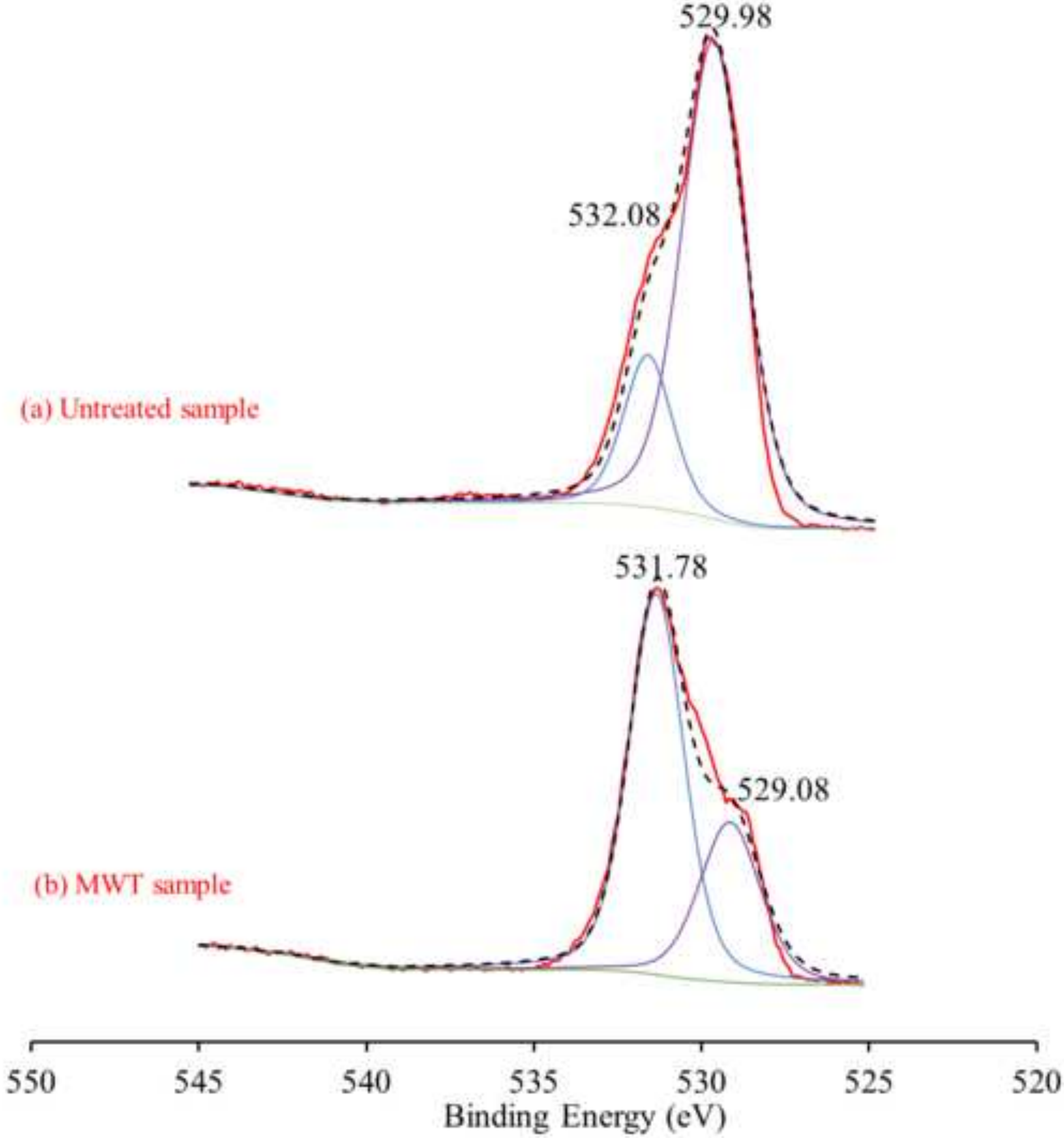
529.98
532.08
(a) Untreated sample
531.78
529.08
(b) MWT sample
550
545
540
535
530
525
520
Binding Energy (eV)

Figure 21

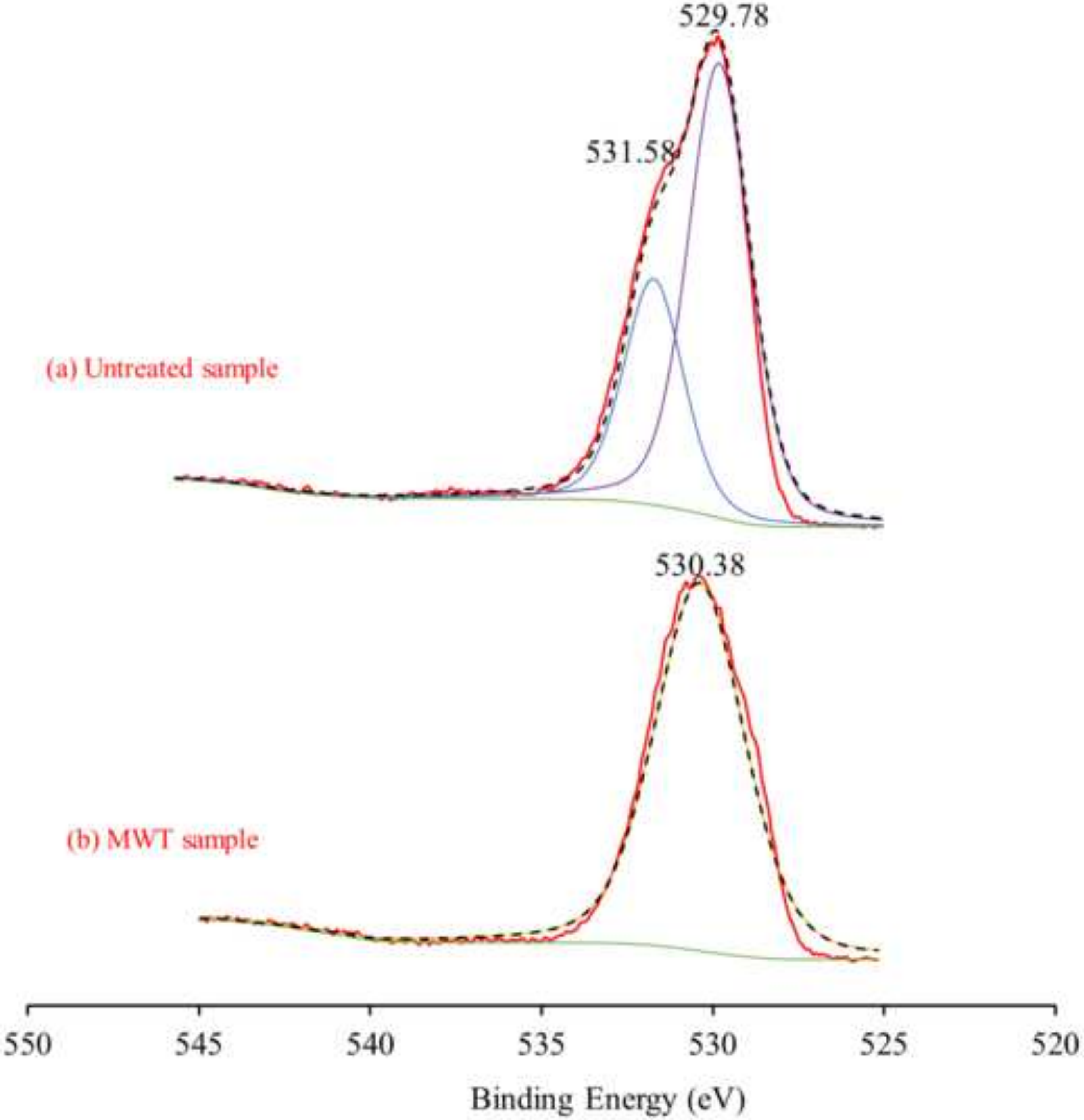
529.78
531.58
(a) Untreated sample
530.38
(b) MWT sample
550
545
540
535
530
525
520
Binding Energy (eV)